Physics – Uspekhi **44** (12) 1229 – 1253 (2001)

REVIEWS OF TOPICAL PROBLEMS PACS numbers: 05.70.Fh, 05.70.Jk, 34.20.Cf, 61.25.Bi, 61.25.Em, 64.70.Dv, 64.70.Fx, 68.10.Cr

Scaling method in atomic and molecular physics

B M Smirnov

DOI: 10.1070/PU2001v044n12ABEH000959

Contents

Abstract. The scaling method based on the parameters of pair atomic interaction potentials proved to be suitable for analyzing the various parameters of dense and condensed rare gases Ne, Ar, Kr, Xe and accurate to within a few percent. In this paper, the interaction potential between radon atoms is evaluated based on the relevant scaling laws and using the macroscopic quantities determining the behavior of dense and condensed gases. Properties of systems of bound particles with a specific pair interaction potential between them are considered, leading to the conclusion that the long-range interatomic interaction is of no significance as far as the properties of dense and condensed rare gases are concerned. Phase transitions in clusters and atomic systems at high pressures are analyzed, and some aspects of scale invariance in dense and condensed molecular systems are under discussion.

1. Introduction

It is well known that a physical quantity of any dimensionality can be constructed on the basis of three typical quantities with different dimensionalities [1]. This provides the basis for various systems of units, which are convenient in a certain branches of science [1 – 3] in spite of the existence of the International System of Units (SI) [4]. Indeed, if we choose a specific system of units for a certain physical object, the parameters of this object are to the order of magnitude of the unit with a given dimensionality for this system of units. Moreover, dimensional analysis can be useful for the determination of some dependences between physical quantities, and this is used widely in hydrodynamics [2, 5, 6] for the analysis of various phenomena. This method becomes more productive if the objects under consideration are similar, and then one can express the parameters of one object through the parameters of the other one. Below we shall analyze the systems of atomic and molecular particles with a pair interaction from this standpoint. Since three-body interactions are weaker in these systems than pairwise ones, this means that the typical interaction energy between neighboring atomic particles in these systems is small compared to an internal energy of an atomic particle. For this reason these systems are gases or condensed media in which atomic particles conserve their individuality in bound systems comprising these particles. The simplest systems with a pair interaction between atoms are rare gases. Molecular gases also relate to these systems.

Evidently, various physical quantities characterizing a system of interacting atomic particles can be expressed through the parameters of the pair interaction potential of particles. A typical interaction potential of two atoms is given in Fig. 1 and is characterized, at least, by two parameters: D, the depth of the potential well, and R_e, the equilibrium distance between the atoms in their diatomic molecule. Considering the behavior of atoms in the system to be classical, we obtain three base parameters m, R_e, D, where m is the atomic mass, so that one can construct any physical parameter of a macroscopic system involving these atoms on the basis of these three parameters. Under this approach we neglect the shape of the atomic interaction potential. In

B M Smirnov Institute for High Temperatures,
Russian Academy of Sciences,
ul. Izhorskaya 13/19, 127412 Moscow, Russian Federation
Tel./Fax (7-095) 190-42 44
E-mail: smirnov@oivtran.iitp.ru

Received 21 February 2001
Uspekhi Fizicheskikh Nauk **171** (12) 1291 – 1315 (2001)
Translated by B M Smirnov; edited by A Radzig

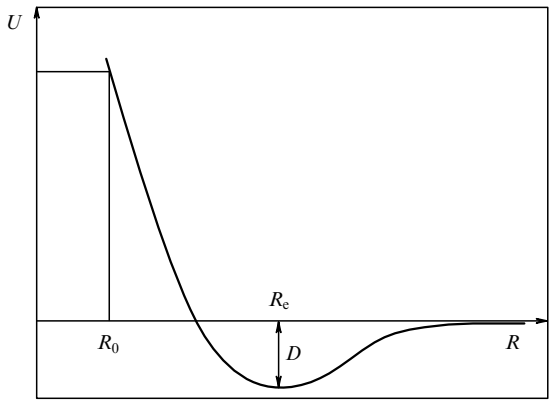

Figure 1. Typical interaction potential of two atoms.

addition, we ignore the long-range interaction between atoms, considering a weak interaction with many surrounding atoms as giving an insignificant contribution to a given macroscopic parameter. Thus, admitting the validity of a scaling law, we neglect some interactions, and the accuracy of these assumptions can be verified from the analysis of the measurable quantities characterizing the system under consideration. This analysis is the goal of the current paper. We make use of information [7 – 14] about various properties of the systems under examination in the analysis of the accuracy of scaling laws and check the validity of the scaling law for some specific properties of the system.

Below we discuss dense and condensed classical inert gases. Along with the check of validity of scaling laws for inert gases, this approach may be useful in two respects. First, it allows us to ascertain the role of a long-range interaction between atoms in such systems. Second, one can understand on this basis the physical character of the properties and phenomena intrinsic to inert gases. Such an analysis can be extended to molecular and complex systems with pair interaction of particles.

2. Dense and condensed rare gases

2.1 Pair interaction potential of rare gas atoms

The parameters of the interaction potential of two inert gas atoms can be found from the analysis of physical quantities which depend on this interaction potential. These quantities are the differential and total cross sections of elastic scattering of two atoms, the second virial coefficient of inert gases, the diffusion coefficient of atoms in the parent inert gas, the thermal conductivity and viscosity coefficients of these gases, the excitation spectra for dimers of inert gas atoms, and some parameters of solid and liquid inert gases. As a result of measurements of these observable quantities and their treatment, reliable parameters of the interaction potential between two atoms of inert gases were found [15 – 18]. Table 1 contains the parameters R_e, the equilibrium distance for the diatomic molecule formed from interacting atoms, and D, the depth of the interaction potential well.

Note that the scaling version under consideration leans upon the parameters of the attractive part of the pair interaction potential of atoms, and hence the parameters of an atomic system are determined by a short-range interaction, when the interaction between nearest neighbors

Table 1. Parameters of the pair interaction potential for rare gas atoms and the reduced parameters of systems consisting of interacting rare gas atoms.

Parameter	Ne	Ar	Kr	Xe
R_e, Å	3.09	3.76	4.01	4.36
D, meV	3.64	12.3	17.3	24.4
D, K	42	143	200	278
m, a.m.u.*	20.18	39.95	83.80	131.3
$p_0 = D/R_e^3$, MPa	20.2	37.1	43.0	47.1
$V_0 = R_e^3$, cm^3 mol^{-1}	17.8	32.0	38.8	49.9
$\rho_0 = m\sqrt{2}/R_e^3$, g cm^{-3}	1.606	1.764	3.051	3.718
C_6, a.u.	6.3	65	130	270
DR_e^6/C_6	0.84	0.90	0.93	1.04
k	7.6	8.1	7.7	5.9
R_0, Å	207	2.85	2.99	3.18

* 1 a.m.u. = 1.6605×10^{-24} g.

dominates in a dense or condensed atomic system. One can construct another version of scaling laws on the basis of a long-range interaction between atoms. Indeed, at large separations R the interaction potential of two atoms has the form

$$U(R) = -\frac{C_6}{R^6}\,. \tag{2.1}$$

where the values of the constants C_6 for two identical atoms of rare gases are compiled in Table 1 [19]. In a new scaling version, we take as the base units m, R_e, C_6, i.e. in the above version we replace the depth of the potential well D by the constant C_6 of a long-range interaction. Table 1 contains the values of the reduced parameter DR_e^6/C_6, and the statistically average value of this parameter is 0.93 ± 0.08, and within the accuracy of several percent both versions may be valid. Nevertheless, below we keep the version leaned upon the short-range character of interatomic interaction, and in the next chapter we prove the validity of this scheme.

The mutual repulsion of interacting atoms at small distances between them is determined by the exchange interaction potential due to overlapping of their atomic electron shells. The corresponding interaction potential between two atoms varies sharply with variation of the distance R between them — that is, the pair interaction potential is approximated by the formula

$$U(R) = U(R_0)\left(\frac{R_0}{R}\right)^k,$$

where we have $k \gg 1$. Table 1 contains the parameters of this formula as applied to inert gases [20], if $U(R_o) = 0.3$ eV.

2.2 Dense rare gases

We now treat the measured parameters of simple systems with a pair interaction of particles from the standpoint of scaling laws. We start from dense rare gases when the interaction between atoms influences the properties of a gas. The popular equation of state for a dense gas is the van der Waals equation [21 – 23] which takes the form

$$\left(p + \frac{n^2 a}{V^2}\right)(V - nb) = nRT\,. \tag{2.2}$$

Here, p is the pressure, V is the volume, T is the temperature, R is the molar gas constant, and n is the amount of gas measured in moles. Below we take $n = 1$, and the molar gas

constant is equal to

$$R = 82.06\,\frac{\mathrm{cm}^3}{\mathrm{mol}}\,\frac{\mathrm{atm}}{\mathrm{K}} = 8.314\,\frac{\mathrm{cm}^3}{\mathrm{mol}}\,\frac{\mathrm{MPa}}{\mathrm{K}}\,.$$

The quantities a, b are the so-called van der Waals constants whose values are presented in Table 2 for rare gases. There are more accurate equations describing the gaseous state [22, 24, 25], but the van der Waals equation is used more often due to its simplicity and since it simultaneously governs the gaseous and liquid states. A scaling analysis allows one to estimate the accuracy of this equation. Indeed, on the basis of this equation one can determine the parameters of the critical point starting from which the liquid and gaseous states are not distinguished. At the critical point we have [23, 26, 27]

$$\left(\frac{\partial p}{\partial V}\right)_T = 0\,, \quad \left(\frac{\partial^2 p}{\partial V^2}\right)_T = 0\,. \tag{2.3}$$

Table 2. Parameters of the van der Waals equation for rare gases [4] and their reduced values.

Parameter	Ne	Ar	Kr	Xe	Average
a, 10^5 MPa cm^6 mol^{-2}	0.208	1.35	2.32	4.19	—
b, cm^3 mol^{-1}	16.72	32.01	39.6	51.56	—
$a/(DR_e^3)$	3.27	3.57	3.59	3.57	3.50 ± 0.15
b/R_e^3	0.941	1.000	1.020	1.033	1.00 ± 0.04
V_{liq}/b	0.97	0.88	0.87	0.83	0.89 ± 0.06

According to the van der Waals equation (2.2), the parameters V_{cr}, p_{cr}, T_{cr} at the critical point are expressed through the constants of this equation as

$$V_{\mathrm{cr}} = 3b\,, \quad p_{\mathrm{cr}} = \frac{a}{27b^2}\,, \quad T_{\mathrm{cr}} = \frac{8a}{27b}\,. \tag{2.4}$$

In particular, this leads to a simple relation between the parameters at the critical point:

$$\frac{T_{\mathrm{cr}}}{V_{\mathrm{cr}}\,p_{\mathrm{cr}}} = \frac{8}{3}\,. \tag{2.5}$$

Table 3 enumerates the critical parameters of rare gases. Notice that the validity of the scaling law for critical parameters within the framework of the scheme under consideration confirms that the critical phenomena in dense rare gases are determined by the attractive interaction of rare gas atoms. One can see that the accuracy of the scaling law for interacting rare gas atoms amounts to several percent. According to the data of Table 3, the ratio $T_{\mathrm{cr}}/p_{\mathrm{cr}}V_{\mathrm{cr}}$ is equal, on average, to 3.4 ± 0.1. Comparing this result with formula (2.5), one can conclude that the exactness of the van der Waals equation of gaseous state is characterized by an accuracy of tens of percent in the range of parameter variation where the interaction of atoms is significant. The state of a system of particles in the given volume is conveniently characterized by the packing density $\varphi = 4\pi r_0^3 N/3$, where $r_0 = R_e/2$ is the particle radius, and N is the particle number density (Table 3 lists values of the factor φ_{cr} relevant to the critical point). For comparison, one obtains $\varphi = \pi\sqrt{2}/6 = 0.7405$ in the case of the crystal incorporating these particles.

Table 3. Critical parameters of rare gases [14] and their reduced values.

Parameter	Ne	Ar	Kr	Xe	Average
T_{cr}, K	44.4	150.9	209.4	289.7	—
p_{cr}, MPa	2.76	4.90	5.50	5.84	—
V_{cr}, cm^3 mol^{-1}	42	75	91	118	—
$\rho_{\mathrm{cr}}/\rho_0$	0.283	0.302	0.302	0.300	0.297 ± 0.009
φ_{cr}	0.209	0.224	0.224	0.222	0.220 ± 0.007
T_{cr}/D	1.05	1.06	1.04	1.02	1.04 ± 0.02
$p_{\mathrm{cr}}R_e^3/D$	0.137	0.132	0.128	0.124	0.130 ± 0.006
V_{cr}/R_e^3	2.50	2.34	2.34	2.36	2.38 ± 0.08
$T_{\mathrm{cr}}/(p_{\mathrm{cr}}V_{\mathrm{cr}})$	3.4	3.5	3.2	3.5	3.4 ± 0.1

According to the Clapeyron formula, the equilibrium pressure $p_{\mathrm{sat}}(T)$ of saturated vapor over plane solid and liquid surfaces is given by the following respective formulas [27, 28]

$$p_{\mathrm{sat}}(T) = p_{\mathrm{sol}} \exp\left(-\frac{\varepsilon_{\mathrm{sol}}}{T}\right), \quad p_{\mathrm{sat}}(T) = p_{\mathrm{liq}} \exp\left(-\frac{\varepsilon_{\mathrm{liq}}}{T}\right), \tag{2.6}$$

where the parameters $\varepsilon_{\mathrm{sol}}$, $\varepsilon_{\mathrm{liq}}$ can be considered as the atomic binding energies for the solid and liquid systems under consideration. Figure 2 depicts the temperature dependence of the saturated vapor pressure of rare gases over solid and liquid plane surfaces, while Table 4 gives the parameters of formulas (2.6) for solid and liquid rare gases near the melting point. Note that the parameters $\varepsilon_{\mathrm{liq}}$, p_{liq} can be found by using the magnitudes of the triple and boiling points, and thus obtained values are close to those of Table 4.

Table 4 also contains the boiling point T_{b} for rare gases, i.e. the temperature values at which the saturated vapor pressure is equal to 1 atm. It is necessary to mark that the boiling point is not a parameter which must satisfy the scaling

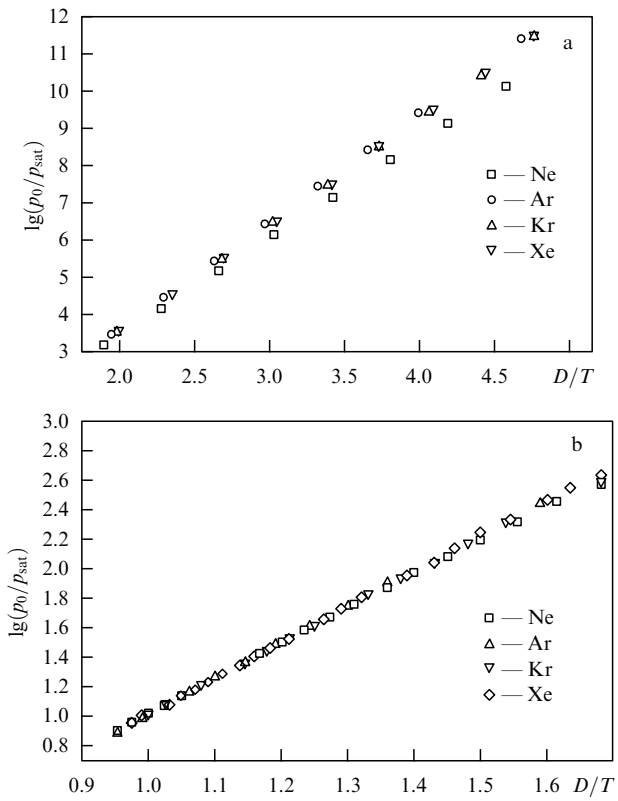

Figure 2. Saturated vapor pressure over the solid (a) and liquid (b) surfaces of rare gases. Experimental data are taken from Ref. [29] for the solid surface, and from Ref. [14] for the liquid phase.

Table 4. Parameters of saturated rare gas vapors over plane solid and liquid surfaces near the melting point.

Parameter	Ne	Ar	Kr	Xe	Average
$\varepsilon_{\rm liq}$, meV	19.4	69.6	95.6	134	—
$p_{\rm liq}$, MPa	410	1060	1030	1270	—
$\varepsilon_{\rm liq}/D$	5.3	5.7	5.5	5.5	5.5 ± 0.1
$p_{\rm liq} R_{\rm e}^3/D$	20	29	24	27	25 ± 4
$\varepsilon_{\rm sol}$, meV	22.5	80.2	112	158	—
$p_{\rm sol}$, MPa	1800	4600	5600	4900	—
$\varepsilon_{\rm sol}/D$	6.2	6.5	6.5	6.5	6.4 ± 0.2
$p_{\rm sol} R_{\rm e}^3/D$	89	124	130	104	110 ± 20
$T_{\rm b}$, K	27.05	87.28	120.1	165.1	—
$T_{\rm b}/D$	0.640	0.610	0.601	0.594	0.61 ± 0.02

law, because it is more correct to compare the temperatures at which the saturated vapor pressure is proportional to a characteristic pressure p_0 for this system, whose values are given in Table 1 for rare gas systems. Comparing the boiling points of various rare gases as temperatures corresponding to different reduced pressures, we get an error in the scaling law, which is estimated to be within the limits of several percent. This error corresponds to the data presented in Table 4.

2.3 Rare gases near the triple point

Solid inert gases have a face-centered cubic crystal lattice [30 – 33]. The hexagonal structure of solid inert gases is only observed in films fabricated on special substrates [34 – 36]. Table 5 lists the parameters of solid inert gases [37, 38], so that a is the distance between nearest neighbors in the crystal lattice at zero temperature, $\rho_0 = \sqrt{2}m/R_{\rm e}^3$, where m is the atomic mass, $\rho(0)$ is the crystal density at zero temperature, $\rho_{\rm sol}$, $\rho_{\rm liq}$ are the densities of the solid and liquid rare gases at the triple point, $T_{\rm tr}$, $p_{\rm tr}$ are the temperature and pressure at the triple point, $\varepsilon_{\rm sub}$ is the binding energy per atom for the solid rare gas at the melting point, $V_{\rm sol}$, $V_{\rm liq}$ are the specific volumes for the solid and liquid states at the melting point, $\Delta S_{\rm fus}$ is the entropy variation as a result of melting at the triple point, $\Delta H_{\rm fus} = T_{\rm tr}\Delta S_{\rm fus}$ is the fusion enthalpy, and $\Delta V = V_{\rm liq} - V_{\rm sol}$ is the volume change as the result of melting. As is seen, the mechanical energy $p_{\rm tr}\Delta V$ released in the course of melting is small in comparison to the fusion enthalpy $\Delta H_{\rm fus}$. This fact allows us to consider the phase transition of rare gases as a thermodynamic process which depends on one variable. The values of the parameter $T_{\rm tr}/(p_{\rm tr}V_{\rm sol})$ show that solid rare gases differ significantly from respective gases for which this parameter is equal to unity.

The behavior of the phase curve of melting, which separates the solid and liquid states, is described near the triple point by the Simon equation [25, 39]

$$\frac{p - p_{\rm tr}}{P} = \left(\frac{T}{T_{\rm tr}}\right)^c - 1\,, \tag{2.7}$$

where $p_{\rm tr}$, $T_{\rm tr}$ are the parameters of the triple point. In Table 5 are given the parameters P and c of this equation [25].

Let us return to equation (2.2). In the course of deduction of this equation we introduced the constant b as the specific volume occupied by atoms. One can take this volume as that relevant to atoms in the liquid state of the atomic system, which is denoted by $V_{\rm liq}$. Table 5 contains corresponding values of the latter, and the ratio $V_{\rm liq}/b$ is given in Table 2. The degree of variation of this ratio from unity testifies to the exactness of the van der Waals equation.

Table 5. Parameters of solid rare gases and their reduced values near the triple point.

Parameter	Ne	Ar	Kr	Xe	Average
a, Å	3.156	3.755	3.992	4.335	—
$a/R_{\rm e}$	1.02	1.00	0.99	1.01	1.005 ± 0.013
$\rho(0)/\rho_0$	1.06	1.00	0.99	0.98	1.01 ± 0.04
$\rho_{\rm sol}$, g cm^{-3}	1.444	1.623	2.826	3.540	—
$\rho_{\rm sol}/\rho_0$	0.899	0.920	0.926	0.952	0.92 ± 0.02
$\rho_{\rm liq}$, g cm^{-3}	1.247	1.418	2.441	3.076	—
$\rho_{\rm liq}/\rho_0$	0.776	0.804	0.800	0.827	0.80 ± 0.02
$\rho_{\rm sol}(0)/\rho_{\rm liq} - 1$	0.159	0.144	0.157	0.151	0.153 ± 0.006
$T_{\rm tr}$, K	24.54	83.78	115.8	161.4	—
$T_{\rm tr}/D$	0.581	0.587	0.578	0.570	0.579 ± 0.007
$p_{\rm tr}$, kPa	43.3	68.8	73.1	81.6	—
$p_{\rm tr}/p_0$, 10^{-3}	2.2	1.9	1.7	1.7	1.9 ± 0.2
$V_{\rm liq}$, cm^3 mol^{-1}	16.2	28.2	34.3	42.7	—
$V_{\rm liq}/R_{\rm e}^3$	0.911	0.879	0.884	0.855	0.88 ± 0.02
$V_{\rm sol}$, cm^3 mol^{-1}	14.0	24.6	29.6	37.1	—
$V_{\rm sol}/R_{\rm e}^3$	0.77	0.77	0.76	0.74	076 ± 0.01
$\varepsilon_{\rm sub}$, meV	22	80	116	164	—
$\varepsilon_{\rm sub}/D$	6.1	6.5	6.7	6.7	6.5 ± 0.3
$\varepsilon_{\rm sub}/\varepsilon_{\rm sol}$	0.98	1.00	1.04	1.04	1.02 ± 0.03
$T_{\rm tr}/(p_{\rm tr}V_{\rm sol})$	340	400	450	450	410 ± 50
$\Delta H_{\rm fus}/D$	0.955	0.990	0.980	0.977	0.98 ± 0.02
$\Delta S_{\rm fus}$	1.64	1.69	1.70	1.71	1.68 ± 0.03
$p_{\rm tr}\Delta V/\Delta H_{\rm fus}$, 10^{-4}	2.8	2.1	2.1	2.0	2.2 ± 0.4
P, MPa	102	209	235	258	—
c	1.600	1.593	1.617	1.589	1.60 ± 0.01
P/p_0	5.14	5.70	5.52	5.52	5.5 ± 0.2

2.4 Liquid rare gases

Let us consider a macroscopic liquid drop. The Wigner – Seitz radius $r_{\rm W}$ for a system of randomly distributed atoms is defined as

$$r_{\rm W} = \left(\frac{3m}{4\pi\rho}\right)^{1/3}, \tag{2.8}$$

where m is the atomic mass, and ρ is the bulk density. In this case the average volume per atom equals $4\pi r_{\rm W}^3/3$. Table 6 collates the values of the Wigner – Seitz radius for liquid rare gases near the triple point. In addition, this table contains the atomic binding energy $\varepsilon_{\rm ev}$ for the liquid state, i.e. the energy which is expended for evaporating one atom at the boiling point.

Table 6. Parameters of liquid rare gases.

Parameter	Ne	Ar	Kr	Xe	Average
$r_{\rm W}/R_{\rm e}$	0.654	0.639	0.641	0.627	0.64 ± 0.01
σ, erg cm^{-2}	5.65	13.55	16.33	18.83	
$\sigma R_{\rm e}^2/D$	0.93	0.97	0.95	0.95	0.94 ± 0.02
A, meV	18.1	61.4	84.8	111	
A/D	4.98	5.00	4.90	4.53	4.9 ± 0.2
$\varepsilon_{\rm ev}$, meV	18.6	68	95	132	
$\varepsilon_{\rm ev}/D$	5.1	5.5	5.5	5.4	5.4 ± 0.2
$\varepsilon_{\rm ev}/\varepsilon_{\rm liq}$	0.96	0.98	0.99	0.98	0.98 ± 0.01
$(\varepsilon_{\rm ev} + \Delta H_{\rm fus})/\varepsilon_{\rm sub}$	1.00	1.00	1.00	0.96	0.99 ± 0.02
q	10.10	10.27	10.11	10.19	10.17 ± 0.08
q'	10.07	10.15	10.14	10.19	10.14 ± 0.04

Figure 3 gives the dependence of the surface tension of liquid rare gases as a temperature function [40, 41], and Table 6 compiles the surface tension of rare gases in the liquid state near the triple point [40, 41]. It is convenient to

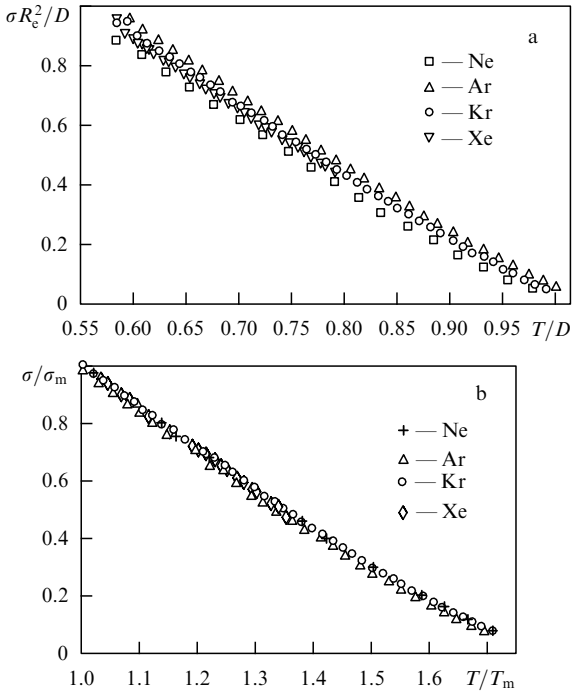

Figure 3. Surface tension of liquid rare gases in the case where this quantity is reduced (a) to the parameters of the pair interaction potential of atoms, and (b) to the surface tension at the melting point. Experimental data are taken from works [40, 41].

introduce the specific surface energy of a bulk liquid drop consisting of n atoms, if we represent the total binding energy E of atoms for this drop in the form of an expansion in terms of the small parameter $n^{-1/3}$. Then we have [42]

$$E = \varepsilon n - An^{2/3}\,, \tag{2.9}$$

where the parameter ε is the binding energy of bulk per atom, and the parameter A is the specific surface energy of this drop. Evidently, for the liquid state the quantity ε is close to the parameters $\varepsilon_{\rm liq}$, $\varepsilon_{\rm ev}$ in formula (2.6) and Table 4. The specific surface energy A is connected with the surface tension σ, so that by definition the surface energy of a surface having an area S is equal to $E_{\rm sur} = \sigma S$. Comparing this relationship with definition (2.9) for the surface energy of the liquid drop of radius r, we arrive at the formula

$$A = \frac{4\pi r^2\sigma}{n^{2/3}} = 4\pi r_{\rm W}^2\sigma\,. \tag{2.10}$$

In Table 6 are given the specific surface energies A for the liquid state of rare gases near the triple point.

It is easy to verify that we have the following relation valid for the phase curve:

$$\varepsilon_{\rm sub} = \varepsilon_{\rm liq} + \Delta H_{\rm fus}\,, \tag{2.11}$$

where $\varepsilon_{\rm sub}$, $\varepsilon_{\rm liq}$ are the binding energies per atom for the solid and liquid states in the melting curve, and this relation can be considered as the definition of the specific fusion energy. Table 6 contains the values of the ratio $(\varepsilon_{\rm ev} + \Delta H_{\rm fus})/\varepsilon_{\rm sub}$, which are equal to one if the quantity $\varepsilon_{\rm ev}$ coincides with the atomic binding energy $\varepsilon_{\rm liq}$ for the liquid state.

One can consider the liquid state of a system with a pair interaction of atoms as a result of formation of voids inside the system [43]. These voids can be thought of as effective vacancies, so that an individual effective vacancy occupies a volume of one atom. Then the relative number of such vacancies can be determined from the variation of the system density as a result of the phase transition. The number of nearest neighbors for an internal atom in the solid-state system of such atoms equals 12, and we denote the average number of nearest neighbors for the liquid state by q. This quantity is equal to [37, 44]

$$q = 24 - \frac{12\rho_{\rm sol}}{\rho_{\rm liq}} \tag{2.12}$$

within the framework of the model involved, where $\rho_{\rm sol}$, $\rho_{\rm liq}$ are the densities for the solid and liquid states of the system. The number of nearest neighbors q of an internal atom, or the coordination number, can be determined from the fusion energy under the assumption of a short-range character of interaction in this system, i.e. if only nearest neighbors interact. Then we obtain for the average number of nearest neighbors:

$$q' = \frac{12\varepsilon_{\rm liq}}{\varepsilon_{\rm sub}} = \frac{12}{1 + \Delta H_{\rm fus}/\varepsilon_{\rm liq}}\,, \tag{2.13}$$

where $\varepsilon_{\rm sub}$, $\varepsilon_{\rm liq}$ are the binding energies per atom for the solid and liquid states, and $\Delta H_{\rm fus}$ is the specific fusion enthalpy.

Table 6 collates the numbers of nearest neighbors q and q' for liquid rare gases, which were determined in accordance to formulas (2.12), (2.13). For their calculations we replaced the atomic binding energy $\varepsilon_{\rm liq}$ in the liquid state at the melting point by the atomic binding energy $\varepsilon_{\rm ev}(T_{\rm b})$ at the boiling point, with a consequent increase in q. As is seen from the data of Table 6, both the methods offer close values of the number of nearest neighbors for liquid inert gases that confirms the validity of this rough model. Averaging the sought-for number over the various inert gases and the methods of its determination, we obtain the following result: $q = 10.15 \pm 0.06$. In addition, from these data it follows that one effective vacancy in the liquid inert gas at the melting point relates to 5.6 ± 0.2 atoms [37].

Above analysis shows that a crude model of liquid as a system consisting of atoms located at sites of the crystal lattice and effective vacancies at certain sites may be useful for the description of some properties of liquid rare gases.

2.5 Classical condition for condensed rare gases

Assuming the scaling laws for rare gases to be valid, we suppose a classical character of atomic movements in dense and condensed gases. For molecules this approach holds true if their typical vibrational energy $\hbar\omega$ is small in comparison to the binding energy of atoms. The relevant criterion has the form $\hbar\omega \ll D$, i.e. the vibrational energy $\hbar\omega$ is small in comparison with the dissociation energy D, and can be written for a diatomic molecule as

$$D^2 \gg \frac{\hbar^2}{m}\,U''\,, \tag{2.14}$$

where m is the atomic mass, $U(R)$ is the interaction potential of two atoms, and the derivative is taken near the bottom of the potential well. This criterion means that the diatomic

molecule must possess many vibrational levels and such a condition is violated for neon and argon diatomics.

For a system of many bound atoms, the classical criterion takes the form

$$\varepsilon_{\rm sub} \gg \theta_{\rm D}\,, \tag{2.15}$$

where $\theta_{\rm D}$ is the Debye temperature for condensed rare gases, and $\varepsilon_{\rm sub}$ is the energy of sublimation, i.e. the energy expended per atom in transformation of a condensed system into a gas. Table 7 contains the Debye temperatures for solid rare gases, and also their sublimation energies taken from Table 4. As is seen, criterion (2.15) is fulfilled.

Table 7. Debye temperature $\theta_{\rm D}$ [33] and separately taken longitudinal $\theta_{\rm D}^{\rm l}$ and transverse $\theta_{\rm D}^{\rm t}$ Debye temperatures [45] for condensed rare gases.

Parameter	Ne	Ar	Kr	Xe
$\theta_{\rm D}$, K	75	92	72	64
$\theta_{\rm D}^{\rm l}$, K	79	100	72	63
$\theta_{\rm D}^{\rm t}$, K	70	69	50	44
$\varepsilon_{\rm sub}$, K	260	930	1300	1900

2.6 Parameters of dense and condensed radon

We now demonstrate the possibilities of the scaling method in regard to evaluating the parameters of the interaction potential between two radon atoms on the basis of some parameters characterizing dense and condensed radon. In Table 8 are listed several parameters pertaining to dense and condensed radon. From these data by relying on the scaling laws for reduced quantities (see Tables 3 – 5) we find for the parameters of the interaction potential of two radon atoms the following values:

$$D = 30.2 \pm 0.4 \text{ meV}, \qquad R_{\rm e} = 4.68 \pm 0.04 \text{ Å}\,.$$

Table 8. Parameters of a system of interacting and bound radon atoms.

Parameter	Value	Reduced value
$T_{\rm tr}$, K	202.1	0.58 ± 0.01
$T_{\rm b}$, K	211.4	0.602 ± 0.007
$T_{\rm cr}$, K	377	1.07 ± 0.01
a, 10^5 MPa cm^6 mol^{-2}	6.6	3.7 ± 0.2
b, cm^3 mol^{-1}	62.4	1.01 ± 0.03
$p_{\rm cr}$, MPa	6.28	0.135 ± 0.006
$\varepsilon_{\rm sol}$, meV	188	6.2 ± 0.1
$\varepsilon_{\rm liq}$, meV	181	6.0 ± 0.1
$p_{\rm liq}$, 10^3 MPa	2.1	45 ± 4

Here the error accounts for the statistical weight of results obtained with different physical quantities. In addition, the scaling approach allows us to determine the other parameters of condensed radon systems:

$$\rho_{\rm liq} = 3.9 \pm 0.2 \text{ g cm}^{-3}\,, \quad \rho_{\rm sol} = 4.5 \pm 0.2 \text{ g cm}^{-3}\,,$$
$$p_{\rm tr} = 90 \pm 20 \text{ MPa}\,, \quad \Delta H_{\rm fus} = 29.6 \pm 1 \text{ meV}\,,$$
$$V_{\rm liq} = 55 \pm 1 \text{ cm}^3 \text{ mol}^{-1}\,, \quad V_{\rm cr} = 149 \pm 6 \text{ cm}^{-3} \text{ mol}^{-1}\,,$$

and we used the same notation as earlier.

In addition, the surface tension of liquid radon near the triple point is $\sigma = 23.0$ erg cm^{-2} [41]. From the above data we find $\sigma R_{\rm e}^2/D = 1.04 \pm 0.03$ for radon, whereas according to the data of Table 6 this value is 0.94 ± 0.02 for other rare gases. This all confirms the conclusion that the accuracy of several percent is achieved when obtaining radon parameters.

2.7 Peculiarities of scaling laws for systems of rare gas atoms

In conclusion of the scaling analysis for rare gas systems we enumerate the factors which cause the scaled parameters to be in error. First, we assume that the character of atomic interaction in dense and condensed systems does not depend on the shape of the pair interaction potential between atoms, so it is only determined by the parameters of the atomic interaction potential near the well bottom. Second, we ignore the contribution of a long-range interaction of atoms to the parameters of the system under consideration. Third, we neglect the quantum effects. Fourth, we assume that three-body interactions of atoms are not of importance for these systems. Evidently, the correctness of these assumptions influences the accuracy of the scaling laws for the rare gas systems. The analysis fulfilled for the example of dense and condensed rare gases shows that the scaling law holds true with the accuracy of several percent.

It is essential that there are several different parameters of the same dimensionality, whose employment allows one to improve the accuracy of the results. Table 9 contains the ratios of the parameters with the similar dimensionality. For the scaling analysis we used the following parameters with the dimensionality of energy: $T_{\rm tr}$, $T_{\rm b}$, $T_{\rm cr}$, $\varepsilon_{\rm ev}$, $\varepsilon_{\rm sub}$ (the notation is coincident with that given above), the quantities $V_{\rm liq}$, $V_{\rm cr}$, b of the volume dimension, the quantities $p_{\rm tr}$, $p_{\rm cr}$ of the pressure dimension, and also the constant a entering into the van der Waals equation. We did not include the quantities $\varepsilon_{\rm liq}$, $\varepsilon_{\rm sol}$ in this list assuming them to be identical to $\varepsilon_{\rm ev}$, $\varepsilon_{\rm sub}$, and the quantities $p_{\rm liq}$, $p_{\rm sol}$ [formula (2.6)] which by definition correspond to a typical number density of atoms and are characterized by a large error. The variety of physical parameters under consideration improves the scaling analysis and excludes random errors from this analysis.

Table 9. Ratios of quantities of an identical dimensionality for dense and condensed rare gases.

Ratio	Ne	Ar	Kr	Xe	Average
$T_{\rm b}/T_{\rm tr}$	1.808	1.801	1.805	1.795	1.802 ± 0.006
$T_{\rm cr}/T_{\rm b}$	1.64	1.73	1.75	1.76	1.72 ± 0.05
$\varepsilon_{\rm liq}/T_{\rm tr}$	9.2	9.6	9.6	9.6	9.5 ± 0.2
$\varepsilon_{\rm sol}/T_{\rm tr}$	10.6	11.2	11.3	11.4	11.1 ± 0.4
$V_{\rm cr}/V_{\rm liq}$	2.74	2.66	2.65	2.76	2.70 ± 0.06
$p_{\rm cr}/p_{\rm tr}$	64	71	75	72	70 ± 5
$\varepsilon_{\rm sol}/T_{\rm cr}$	5.9	6.2	6.2	6.3	6.2 ± 0.2
$\varepsilon_{\rm liq}/T_{\rm cr}$	5.1	5.4	5.3	5.4	5.3 ± 0.1
$\varepsilon_{\rm ev}/T_{\rm cr}$	4.9	5.2	5.3	5.3	5.2 ± 0.2
$\varepsilon_{\rm ev}/\varepsilon_{\rm liq}$	0.96	0.98	0.99	0.98	0.98 ± 0.01
$V_{\rm cr}/V_{\rm liq}$	2.74	2.66	2.65	2.76	2.70 ± 0.06
$V_{\rm cr}/b$	2.51	2.34	2.30	2.29	2.36 ± 0.10
$p_{\rm cr}/p_{\rm tr}$	64	71	75	72	70 ± 5
$T_{\rm cr}R_{\rm e}^6/C_6$	0.89	0.95	0.97	1.06	0.97 ± 0.07

Figure 4 illustrates the phase diagram of rare gases, and we indicated on this diagram the domains which were used for the scaling analysis. We apply to the parameters of the triple point ($T_{\rm tr}$, $p_{\rm tr}$, $V_{\rm sol}$, $V_{\rm liq}$) and the critical point ($T_{\rm cr}$, $p_{\rm cr}$, $V_{\rm cr}$). Next, we use the parameters of the three curves of phase coexistence, which include P, c — the parameters of the Simon equation (2.7) for the solid – liquid phase transition,

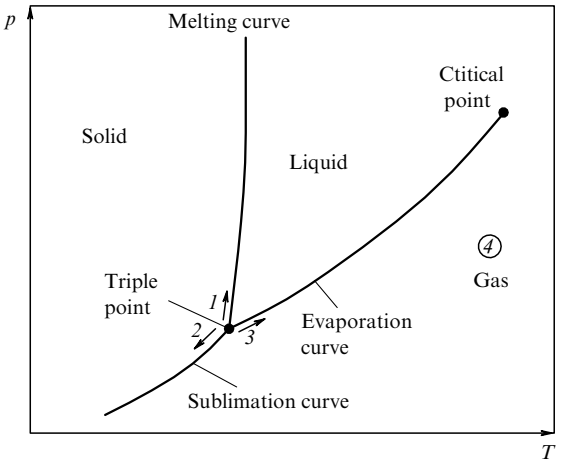

Figure 4. Phase diagram of rare gases and regions of the phase diagram used for the scaling analysis. Namely, the parameters are taken of the triple and critical points, the parameters of phase boundaries near the triple point (*1*, *2*, *3*), and the constants of the van der Waals equation related to the gaseous state (*4*).

and the parameters $\varepsilon_{\rm sol}$ and $\varepsilon_{\rm liq}$ for the solid – gas and liquid – gas phase transitions. The binding energies per atom, $\varepsilon_{\rm sub}$ and $\varepsilon_{\rm ev}$, for the solid and liquid states are assumed to be close to the quantities $\varepsilon_{\rm sol}$ and $\varepsilon_{\rm liq}$, correspondingly. In addition, we use the constants a and b of the van der Waals equation which describes the behavior of a gas of weakly interacting atoms. It is essential that the number of the parameters used significantly exceeds three — the number of parameters on the basis of which a system of measurement units can be constructed. The variety of physical parameters under consideration improves the reliability of the above scaling analysis and excludes occasional errors from this analysis. This fact also allows us to estimate its accuracy that may amount to as much as several percent.

The scaling version employed in our analysis is valid if the parameters appropriate for the domains of the phase diagram in Fig. 4 are determined by the short-range part of the interaction potential between two atoms. This scaling version assumes that the interaction of nearest neighbors gives the main contribution to the energy of the system. Another version can be based on the long-range part of the pair interaction potential (2.1). For demonstration of this possibility, Table 9 gives the reduced critical temperature of rare gases for this scaling version. From this it follows that such a version may also be realized with an accuracy of several percent. Thus, it is necessary to prove the validity of the scaling version under consideration. We shall dwell on this problem in the next section.

3. Systems with a specific particle interaction potential

3.1 The solid state of a system of interacting atoms

In the previous section we analyzed the character of scaling laws for dense and condensed rare gases. As a result, this analysis proved the validity of the similarity laws for various parameters of rare gases with the accuracy of several percent and allowed us to restore unknown parameters on the basis of the scaling procedure. Along with this, the scaling method gives the possibility of ascertaining the nature of various properties of dense and condensed gases if we compare their reduced parameters with those of similar systems with a specific pair interaction potential between their particles. Below we shall consider some properties of atomic systems with a pair interaction potential in order to connect the latter with macroscopic parameters of these systems.

We first consider solids consisting of atoms with a pair interaction potential. If the short-range interaction of atoms gives a significant contribution to the atomic binding energy of the system with a pair interaction of atoms, the solid state of this system of atoms features a close-packed structure. Note that the definition of a short-range interaction in atomic physics [46] differs from that in nuclear physics [47, 48]. Indeed, in nuclear physics a short-range interaction potential is not zero, if the coordinates of interacting particles coincide. A presence of the short-range interaction potential in atomic physics means that in a system of atomic particles the interaction takes place between nearest neighbors only.

We shall model the atoms in this bound system by balls of a radius a, where a is the distance between nearest neighbors. The close-packed structure of balls can be either face-centered cubic (fcc) or hexagonal. Each atom-ball of these structures is surrounded by 12 nearest neighbors. In order to understand the general peculiarities and differences between these two close-packed structures, let us construct them by leaning upon the same method (see Fig. 5). Assuming the atoms to be balls, arrange them on the xy plane in such a way that these balls are placed in parallel lines directed parallel to the x axis. Then neighboring lines are placed at a distance $b = a\sqrt{3}/2$, and the ball center in the next line is shifted with respect to the previous one by a distance $\pm a/2$. Each atom on the plane has 6 nearest neighbors which form a regular hexagon with the side a. This plane is denoted by $\{111\}$.

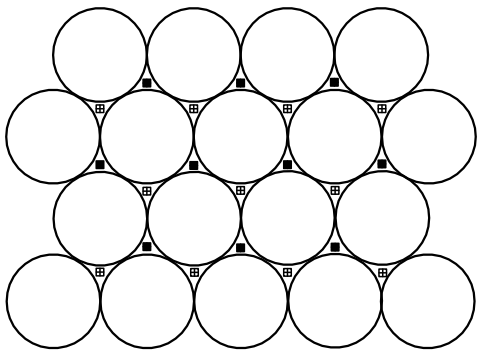

Figure 5. Crystal lattices of close-packed structures. Large circles correspond to positions of atoms-balls of a given layer. Crosses stand for the positions of atomic centers of the previous layer, open squares mark the positions of atomic centers of the subsequent layer for the hexagonal crystal lattice, and filled squares are those for the face-centered cubic lattice.

Let us compose the next plane of balls along the z-axis at a distance of $a\sqrt{2/3}$ from the previous one in such a way that the balls of the next plane are placed in hollows between balls of the previous plane. Then the projections of the balls of the upper plane are shifted in the y-direction with respect to the balls of the preceding plane by a distance $a/\sqrt{3}$.

Up to now the above procedure has related to the construction of both the hexagonal and fcc lattices. Placing balls of the third plane in the hollows of the second plane, we

are led to two types of ball positions (see Fig. 5). If the projections of the balls of the first and third planes coincide, a hexagonal lattice is formed. The other possibility of locating the atoms of the third layer leads to the formation of an fcc lattice. One can see that the number density of balls for both the close-packed structures is equal to $\sqrt{2}/a^3$. Thus, there are two close-packed structures, face-centered cubic and hexagonal, and from the standpoint of interaction character in the system the difference between these structures is minor. Below we shall evaluate the binding energy for these structures for several specific pair interaction potentials. Comparison of real parameters of rare gases with calculated ones will allow us to determine the character of atomic interactions in real solid rare gases.

Placing a test atom at the origin of the coordinates, one can distribute other atoms of the solid system over shells, so that the distance of atoms of one shell from a test atom is identical and atoms belonging to a certain shell can be transformed one into another as a result of transformations which leave this lattice unchanged. Table 10 collates the parameters of atomic shells for the face-centered cubic structure, and Table 11 gives the analogous parameters for the hexagonal structure [44, 49]. Evidently, the binding energy per atom for a system with a pair interaction of atoms is given by [50]

$$\varepsilon_{\text{sub}} = \frac{1}{2}\sum_k n_k U(r_k)\,, \tag{3.1}$$

Table 10. Shell parameters of the fcc-crystal structure, so that r_k is the k-shell distance from a test atom, a is the distance between nearest neighbors, and n_k is a number of shell atoms [44, 49].

Shell	r_k^2/a^2	n_k	Shell	r_k^2/a^2	n_k
011	1	12	044	16	12
002	2	6	334	17	24
112	3	24	035	17	24
022	4	12	006	18	6
013	5	24	244	18	24
222	6	8	116	19	24
123	7	48	235	19	48
004	8	6	026	20	24
114	9	24	145	21	48
033	9	12	226	22	24
024	10	24	136	23	48
233	11	24	444	24	8
224	12	24	055	25	12
015	13	24	017	25	24
134	13	48	345	25	48
125	15	48	046	26	24

where $U(r_k)$ is the interaction potential between an atom of the kth shell and a test atom, and the numerical factor 1/2 accounts for the fact that each bond relates to two atoms.

It is convenient to divide the specific binding energy into three parts [51]:

$$\varepsilon_{\text{sub}} = \varepsilon_{nn}(R_{\text{e}}) + \varepsilon_{nnn}(R_{\text{e}}) + \varepsilon_{\text{str}}\,, \tag{3.2}$$

where $\varepsilon_{nn}(R_{\text{e}})$, $\varepsilon_{nnn}(R_{\text{e}})$ are the interaction energies between nearest neighbors and non-nearest neighbors, respectively, and the strain energy is given by

$$\varepsilon_{\text{str}} = \varepsilon_{\text{sub}}(a) - \varepsilon_{\text{sub}}(R_{\text{e}})\,, \tag{3.3}$$

where a is the optimal distance between nearest neighbors, which corresponds to the maximum binding energy in the crystal. For the close-packed structures, $\varepsilon_{nn}(R_{\text{e}}) = 6D$. In the case of a short-range interaction between atoms, if only nearest neighbors interact, we have $\varepsilon_{nn}(R_{\text{e}}) = 6D$, $\varepsilon_{nnn} = \varepsilon_{\text{str}} = 0$, and

$$\varepsilon_{\text{sub}} = 6D\,, \quad a = R_{\text{e}}\,. \tag{3.4}$$

From the data of Table 5 it follows that the sublimation energy and the distances between nearest neighbors in solid rare gases are close to those of a system with a short-range atomic interaction.

Table 11. Shell parameters of the hexagonal crystal structure, so that r_k is the distance of atoms of the kth shell from a test atom, a is the distance between nearest neighbors, and n_k is a number of shell atoms [44, 49].

Layer	r_k^2/a^2	n_k	Layer	r_k^2/a^2	n_k
0	1	6	1	9	6
1	1	6	2	29/3	24
1	2	6	1	10	12
2	8/3	2	3	31/3	12
0	3	6	4	32/3	2
1	3	12	1	11	12
2	11/3	12	3	34/3	6
0	4	6	2	35/3	12
1	5	12	4	35/3	12
2	17/3	12	0	12	6
1	6	6	3	37/3	12
3	19/3	6	0	13	12
2	20/3	12	1	13	12
0	7	12	4	41/3	12
1	7	12	3	43/3	6
3	22/3	6	2	44/3	12
3	25/3	12	4	44/3	12
0	9	6	1	15	12

3.2 Lennard – Jones crystal and gas

We now consider the other types of pair interaction potential between atoms in order to ascertain the role of a long-range interatomic interaction in the formation of real crystals. The most popular Lennard – Jones potential of pair interaction between atoms assumes the form

$$U_{\text{LD}}(R) = D\left[\left(\frac{R_{\text{e}}}{R}\right)^{12} - 2\left(\frac{R_{\text{e}}}{R}\right)^{6}\right], \tag{3.5}$$

where R is the distance between atoms. This interaction potential is often taken as an accurate potential describing interaction of two atoms of rare gases [33, 52], and we shall show that such an inference is incorrect. Below we shall determine the sublimation energy of the Lennard – Jones crystal. Then formula (3.1) gives for the specific sublimation energy of the crystal [33] the following expression

$$\frac{\varepsilon_{\text{sub}}}{D} = -\frac{C_1}{2}\left(\frac{R_{\text{e}}}{a}\right)^{12} + C_2\left(\frac{R_{\text{e}}}{a}\right)^{6},$$
$$C_1 = \sum_k n_k\left(\frac{R_{\text{e}}}{r_k}\right)^{12}, \quad C_2 = \sum_k n_k\left(\frac{R_{\text{e}}}{r_k}\right)^{6}. \tag{3.6}$$

Optimizing formula (3.6), we arrive at the optimal distance a between nearest neighbors and the specific binding energy ε_{sub}:

$$a = R_{\text{e}}\left(\frac{C_1}{C_2}\right)^{1/6}, \quad \varepsilon_{nn} = 6D\,, \quad \varepsilon_{nnn} = \left(C_2 - \frac{C_1}{2} - 6\right)D\,,$$
$$\varepsilon_{\text{str}} = \frac{(C_2 - C_1)^2}{2C_1}D\,, \quad \varepsilon_{\text{sub}} = \frac{C_2^2 D}{2C_1}\,. \tag{3.7}$$

Replacing the summation in formula (3.6) by integration for $R \geqslant r_0$, we find the contribution to the constants C_1, C_2 from an atomic domain where $r_k > r_0$:

$$\Delta C_1 = \frac{1}{2}\sum_{R \geqslant r_0} \frac{n_k}{r_k^{12}} = \frac{1}{2}\int_{r_0}^{\infty} \frac{\sqrt{2}}{a^3}\,\frac{4\pi r^2\,\mathrm{d}r}{r^{12}} = \frac{4\pi\sqrt{2}}{9r_0^9}\,,$$

$$\Delta C_2 = \sum_{R \geqslant r_0} \frac{n_k}{r_k^{6}} = \int_{r_0}^{\infty} \frac{\sqrt{2}}{a^3}\,\frac{4\pi r^2\,\mathrm{d}r}{r^{6}} = \frac{4\pi\sqrt{2}}{3r_0^3}\,.$$

We now account for the fact that the average number density of atoms in a close-packed crystal structure is $\sqrt{2}/a^3$. Choosing r_0^2 to be between 26 and 27, we get the following results for the face-centered cubic structure of the crystal on the basis of the data from Table 10 [33]:

$$C_1 = 12.131\,, \quad C_2 = 14.454 \pm 0.002\,,$$

and the error indicated is caused by the choice of the lower limit of integration. In the expressions for ΔC_1, ΔC_2, we took k_0 such that $r_0^2 = 26$. This gives for the parameters of the Lennard–Jones face-centered cubic crystal (i.e. for a crystal with the Lennard–Jones interaction potential of atoms):

$$a = 0.971 R_\mathrm{e}\,, \quad \varepsilon_\mathrm{sub} = \frac{C_2^2 D}{2C_1} = 8.61 D\,. \tag{3.8}$$

Comparison with formula (3.4) shows that a short-range interaction between atoms makes a contribution of approximately 70% to the energy of the Lennard–Jones crystal with the face-centered cubic structure. Partition of the specific binding energy ε_sub into three parts in accordance with formula (3.7) results in the following expressions for these terms:

$$\varepsilon_{nn}(R_\mathrm{e}) = 6D\,, \quad \varepsilon_{nnn}(R_\mathrm{e}) = \left(C_2 - \frac{C_1}{2} - 6\right)D = 2.39D\,,$$

$$\varepsilon_\mathrm{str} = \frac{(C_2 - C_1)^2}{2C_1} D = 0.22D\,. \tag{3.9}$$

Repeating these operations for the hexagonal lattice, we obtain using the data from Table 11 for parameters of the Lennard–Jones crystal:

$$C_1 = 12.132\,, \quad C_2 = 14.454 \pm 0.002\,.$$

As is seen, within the accuracy of the analysis, the energy parameters of the Lennard–Jones crystal coincide for the fcc and hexagonal structures. Though more accurate calculations show the preferableness of the hexagonal structure [53], this fact has no practical significance.

Comparing the reduced parameters of the Lennard–Jones crystal, obtained according to formula (3.8), with those for solid rare gases (see Table 5), we convince ourselves that the Lennard–Jones interaction potential is not suitable for condensed rare gases. This inference also relates to other parameters of the Lennard–Jones system [54, 55]. The reduced temperature of the Lennard–Jones system at the triple point is $T_\mathrm{tr}/D = 0.695$; the reduced density of the liquid Lennard–Jones system is $\rho_\mathrm{liq}/\rho_0 = 0.85$ at the triple point. The reduced parameters for the critical point are as follows: $V_\mathrm{cr}/R_\mathrm{e}^3 = 2.33$, $T_\mathrm{cr}/D = 1.316$, and $p_\mathrm{cr}R_\mathrm{e}^3/D = 0.184$. The critical parameters are equal to $V_\mathrm{cr}/R_\mathrm{e}^3 = 2.9 \pm 0.2$, and $T_\mathrm{cr}/D = 1.34 \pm 0.02$ [56, 57]. As is seen, the values of the above parameters at the critical point, except the critical volume, differ from those of rare gases (see Tables 3, 5). In addition, the ratio $T_\mathrm{cr}/(p_\mathrm{cr}V_\mathrm{cr})$ is 3.1 for the Lennard–Jones system that differs from 3.4 ± 0.1 (Table 3) for rare gases. All this permits one to conclude that the Lennard–Jones interaction potential does not describe rare gases.

3.3 Morse crystal

The other type of interaction potential allows us to vary the ratio between the short-range and long-range parts of the interaction potential. We now consider a crystal consisting of atoms with a Morse interaction potential which takes the form

$$U(R) = D\Big\{\exp\left[2\alpha(R - R_\mathrm{e})\right] - 2\exp\left[\alpha(R - R_\mathrm{e})\right]\Big\}\,, \tag{3.10}$$

and passes a minimum at $R = R_\mathrm{e}$. According to formula (3.1), we have for the specific binding energy of crystal atoms:

$$\varepsilon_\mathrm{sub} = D\left[\exp(\alpha R_\mathrm{e})F(\alpha a) - \frac{1}{2}\exp(2\alpha R_\mathrm{e})F(2\alpha a)\right]\,,$$

$$F(\alpha a) = \sum_k n_k \exp(-\alpha r_k)\,. \tag{3.11}$$

Here, r_k is the distance between a test atom and atoms of the kth shell, n_k is the number of atoms in this shell, and a is the distance between nearest neighbors in the lattice. Values of the function $F(\alpha a)$ may be evaluated on the basis of the data from Table 10 for the face-centered cubic lattice and are compiled in Table 12. In addition, the latter table contains an effective number $F(\alpha a)\exp(\alpha a)$ of atoms that partake in the interactions with a test atom, and the derivative of the function under consideration is given by

$$F'(\alpha a) = \frac{\mathrm{d}F}{\mathrm{d}(\alpha a)} = -\sum_k \frac{n_k r_k}{a}\exp(-\alpha r_k)\,. \tag{3.12}$$

Note that the quantity $F(\alpha a)\exp(\alpha a)$ at large αa tends to 12, i.e. the number of nearest neighbors.

Table 12. Parameters of the face-centered cubic crystal in the case of the Morse interaction potential between atoms [44, 58].

αa	αR_e	$F(\alpha a)$	$-\mathrm{d}F(\alpha a)/\mathrm{d}(\alpha a)$	$F(\alpha a)\exp(\alpha a)$	$\varepsilon_\mathrm{sub}/D$
2	3.03	3.87	6.47	28.6	21.3
3	3.57	0.910	1.17	18.3	12.2
4	4.31	0.274	0.311	14.9	8.94
5	5.17	0.0911	0.0975	13.5	7.52
6	6.10	0.0318	0.0330	12.8	6.84
7	7.06	0.0114	0.0116	12.5	6.47
8	8.03	0.00412	0.00417	12.3	6.29
9	9.02	0.001503	0.001514	12.2	6.18
10	10.01	5.499×10^{-4}	5.523×10^{-4}	12.1	6.11

Formula (3.11) establishes the connection between the equilibrium distance R_e of atoms in the diatomic molecule and the distance a between the nearest neighbors in the crystal. This connection takes the form

$$\exp(\alpha R_\mathrm{e}) = f(\alpha a) = \frac{F'(\alpha a)}{F'(2\alpha a)}\,, \tag{3.13}$$

and the optimal specific binding energy of the crystal is given by

$$\frac{\varepsilon_{\text{sub}}}{D} = f(\alpha a)\, F(\alpha a) - \frac{1}{2} f^2(\alpha a)\, F(2\alpha a)\,. \tag{3.14}$$

These parameters for the lattice of the fcc crystal are given in Table 12.

Notice that in contrast to the Lennard – Jones interaction potential, in the case of the Morse interaction potential between atoms the variation of the free parameter α allows us to change continuously the specific atomic binding energy in the crystal. In particular, the specific binding energy of the Lennard – Jones crystal with the parameters (3.8), $\varepsilon_{\text{sub}} = 8.61D$, is realized at the value of $\alpha a = 4.17$ for the Morse interaction potential. This corresponds to $\alpha R_{\text{e}} = 4.46$, i.e. $a = 0.935R_{\text{e}}$. As is seen, the Morse crystal for this Morse parameter is more compressed than the Lennard – Jones one. In addition, in this case the separate terms of formula (3.2) for the Morse interaction potential of atoms are as follows:

$$\varepsilon_{nn}(R_{\text{e}}) = 6D\,, \quad \varepsilon_{nnn}(R_{\text{e}}) = 2.136D\,, \quad \varepsilon_{\text{str}} = 0.474D\,.$$

The contributions to the total binding energy from interactions between non-nearest neighbors and from the strain energy for the Morse crystal are equal to 25% and 5.5%, correspondingly. For the Lennard – Jones crystal, appropriate values according to formula (3.9) are equal to 28% and 2.6%. From this fact and the crystal compression one may conclude that the crystal parameters depend on the shape of the interaction potential between atoms.

If we approximate the interaction potential of rare gas atoms by the Morse potential, in order to obtain the sublimation energy and the distance between nearest neighbors in accordance with the data of Table 5, it is necessary to take the Morse parameter $\alpha R_{\text{e}} = 8 \pm 1$. In this case the contribution of the interaction between non-nearest neighbors to the total crystal energy is less than 10%. Thus, comparing the crystal parameters of the close-packed structure with those of rare gas solids, one can infer that interaction in solid rare gases is close to being short-range.

3.4 Surface energy of Lennard – Jones and Morse crystals

We now determine the specific surface energy of a crystal with face-centered cubic lattice using the above interaction potentials of atoms. Such a crystal possesses surfaces of three structural types, as is illustrated in Fig. 6. Let us take an infinite fcc crystal and divide it into two parts by a plane {100} or {111}. The specific surface energy corresponds to the interaction potential of these parts per unit area. Let us denote the interaction energy of a test surface atom with all the atoms of the kth layer by ε_k (this atom is located in the zeroth layer). Then the specific surface energy is written as

$$\sigma = \sum_{k=1}^{\infty} \frac{k\varepsilon_k}{s}\,, \tag{3.15}$$

where s is the area per atom, and we took into account that each bond relates to two atoms. From this formula we obtain for the specific surface energy of a solid in the case of the Lennard – Jones interaction potential:

$$\frac{\sigma}{D} = \frac{1}{s}\left(B_6 \frac{R_{\text{e}}^6}{a^6} - B_{12} \frac{R_{\text{e}}^{12}}{2a^{12}}\right), \tag{3.16}$$

where D is the dissociation energy of the diatomic molecule, a is the distance between nearest neighbors, R_{e} is the equilibrium atomic separation, s is the surface area per atom, and

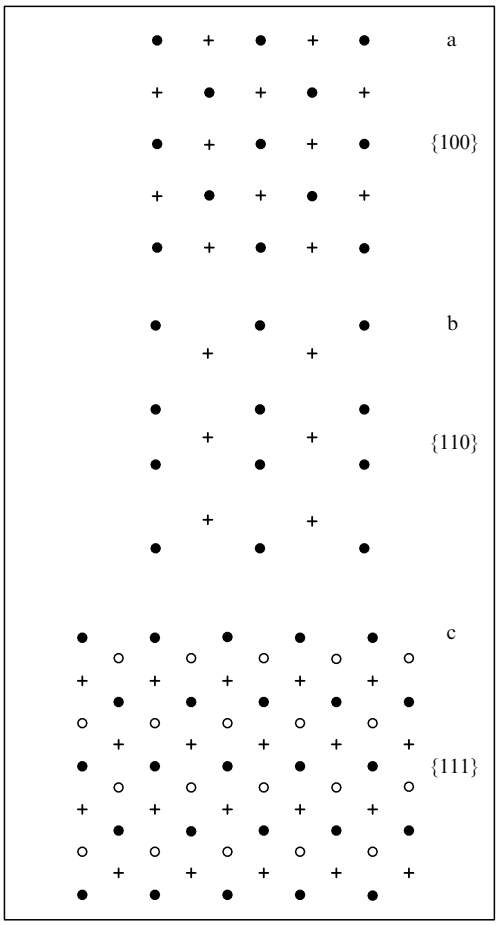

Figure 6. Structural types of surfaces for the fcc crystal with the following directions: (a) {100}; (b) {110}, and (c) {111}. Crosses and open and filled circles relate to different layers.

$$B_6 = \sum_{i,k} k n_{ik} \frac{a^6}{r_{ik}^6}\,, \quad B_{12} = \sum_{i,k} k n_{ik} \frac{a^{12}}{r_{ik}^{12}}\,. \tag{3.17}$$

Here, r_{ik} is the distance from a test atom to the ith atom of the kth layer, and n_{ik} is the number of such atoms.

First we consider the surface {100}. The area per atom of this surface is equal to $s = a^2$, and the distance between neighboring layers is $a/\sqrt{2}$. Table 13 contains information about the numbers of atoms whose distances from a test atom are $r_{ik}^2 \leqslant 12$, and their locations in the layers. We take the sums in formulas (3.17) up to $r_{ik}^2 = 12$, and for $r_{ik}^2 > 12$ we replace the sum by integration both for atoms of the first four layers and atoms of subsequent layers. Correspondingly, the sums in formulas (3.17) reduce to three terms:

$$B_6^{100} = 5.35 + 10a^6 \int_{r_0}^{\infty} \frac{2\pi\rho\, \mathrm{d}\rho\, \mathrm{d}z}{(\rho^2 + z^2)^3} + \sum_{k=5}^{\infty} k a^4 \int_{ka/\sqrt{2}}^{\infty} \frac{2\pi\rho\, \mathrm{d}\rho}{(\rho^2 + k^2 a^2)^3} = 5.39\,,$$

where we took $r_0^2 = 13$. In the same way we get $B_{12}^{100} = 4.06$.

We use the same method for the surface {111}. Table 14 lists relative positions of the nearest atoms for a test atom of

Table 13. Distances between nearest atoms and a test atom of the {100} surface in the fcc crystal [44, 58].

r_{ik}^2/a^2	1st layer	2nd layer	3rd layer	4th layer
1	4	—	—	—
2	—	1	—	—
3	8	4	—	—
4	—	4	—	—
5	4	—	4	—
6	—	4	—	—
7	8	8	8	—
8	—	—	—	1
9	8	—	4	4
10	—	4	—	4
11	—	—	8	—
12	—	8	—	4

Table 14. Distances between nearest atoms and a test atom of the {111} surface in the fcc crystal [44, 58].

r_{ik}^2/a^2	1st layer	2nd layer	3rd layer	4th layer
1	3	—	—	—
2	3	—	—	—
3	6	3	—	—
4	—	3	—	—
5	6	6	—	—
6	3	—	1	—
7	6	6	6	—
8	—	3	—	—
9	3	6	6	—
10	6	—	—	—
11	6	3	6	3
12	—	6	3	3

this surface. In this case we get

$$B_6^{111} = 4.116 + \frac{10\pi}{\sqrt{3}}\,\frac{a^4}{r_0^4} + \frac{3\sqrt{3}\pi}{8k_0^2} = 4.44\,, \quad B_{12}^{111} = 3.07\,,$$

where $k_0 = 5$.

Let us take the distance between nearest neighbors at the surface in the same manner as in the Lennard–Jones crystal: $a = 0.975R_e$. Then, taking into account that for the {100}-surface the area per atom is $s = a^2$, and that for the {111}-surface it is $s = a^2\sqrt{3}/2$, we get from formula (3.17) for the specific surface energy of the appropriate layers the results as follow:

$$\sigma_{100} = \frac{3.66D}{a^2}\,, \quad \sigma_{111} = \frac{3.59D}{a^2}\,. \tag{3.18}$$

In the case of the Morse interaction potential between atoms (3.10), the specific surface energies of the face-centered cubic lattice are given by

$$\sigma = D\left[\exp(\alpha R_e)G(\alpha a) - \frac{1}{2}\exp(2\alpha R_e)G(2\alpha a)\right],$$
$$G(\alpha a) = \sum_{i,k} \frac{kn_{ik}\exp(-\alpha r_{ik})}{s}\,. \tag{3.19}$$

Here, k is the number of a layer, i is the number of an atom in this layer, n_{ik} is a number of such atoms, r_{ik} is the distance from a test surface atom to these atoms, and s is the area per atom in the layer of the corresponding direction. The first terms of this series for the {100}- and {111}-surfaces have the form

$$G_{100} = 4\exp(-\alpha a) + 2\exp(-\alpha a\sqrt{2}) + 16\exp(-\alpha a\sqrt{3}) + 8\exp(-2\alpha a) + 16\exp(-2\alpha a\sqrt{5})\,,$$

$$G_{111} = 3\exp(-\alpha a) + 3\exp(-\alpha a\sqrt{2}) + 12\exp(-\alpha a\sqrt{3}) + 6\exp(-2\alpha a) + 18\exp(-\alpha a\sqrt{5})\,,$$

with the first term of each expansion corresponding to a short-range interaction, i.e. it accounts for the interaction between nearest neighbors only.

The results of numerical calculations are presented in Table 15, with the above sum being restricted to distances $r_{ik}^2 \leqslant 12$. In order to estimate the accuracy of this operation, when we neglected the interaction between a test and farther atoms, we compare the contribution of farther atoms to the sum ΔG with that from nearest neighbors of the first layer, $G_{nn} = n_1\exp(-\alpha a)$, where n_1 is the number of nearest neighbors of a test surface atom in the first layer. Its value would run to $n_1 = 4$ for the {100}-surface plane, and $n_1 = 3$ for the {111}-surface plane. We have in the limit $\alpha r_0 \gg 1$ that

$$\frac{\Delta G}{G_{nn}} = \frac{231}{\beta\alpha n_1}\exp(-2.6\alpha a)$$

for $r_0 = \sqrt{13}$. In particular, for $\alpha a = 3$ and for the {111} surface plane this ratio is 0.01. Because we are guided by the inequality $\alpha a \geqslant 3$, below we shall neglect ΔG.

Table 15. Parameters of a bulk crystallite with the fcc structure for the Morse interaction potential between atoms [44, 58].

αa	αR_e	G_{100}	G_{111}	g_{100}	g_{111}	A	δ_{opt}
2	3.03	2.00	1.70	37.6	32.1	155	0.30
3	3.57	0.387	0.321	11.3	9.52	46.4	0.33
4	4.31	0.103	0.0832	5.53	4.57	22.4	0.35
5	5.17	0.0322	0.0255	3.64	2.94	14.5	0.39
6	6.10	0.0109	$0.0^2$850	2.85	2.28	11.3	0.41
7	7.06	$0.0^2$384	$0.0^2$296	2.48	1.95	9.69	0.43
8	8.03	$0.0^2$138	$0.0^2$106	2.25	1.74	8.71	0.45
10	10.01	$0.0^3$184	$0.0^3$139	2.08	1.59	7.96	0.48
12	12.00	$0.0^4$247	$0.0^4$186	2.02	1.52	7.66	0.49

From above results one can find the specific energy per surface atom:

$$g(\alpha a) = \exp(\alpha R_e)G(\alpha a) - \frac{1}{2}\exp(2\alpha R_e)G(2\alpha a)\,,$$
$$\sigma(\alpha a) = \frac{Dg(\alpha a)}{s}\,,$$

where s is the surface area per atom.

We now apply to the above results for determining the surface energy of solids with face-centered cubic structure. A geometric figure of such a structure with the maximum binding energy of atoms has plane facets with directions {111} and {100} (the definition of such planes is illustrated in Fig. 6), i.e. this figure possess 8 facets as hexagons of the direction {111}, and 6 facets as squares of the direction {100}. This figure is represented in Fig. 7 [59]. One can introduce the total binding energy E of atoms in this system on the basis of formula (2.8), which has the form [42]

$$E = \varepsilon_{sub}n - An^{2/3}\,, \tag{3.20}$$

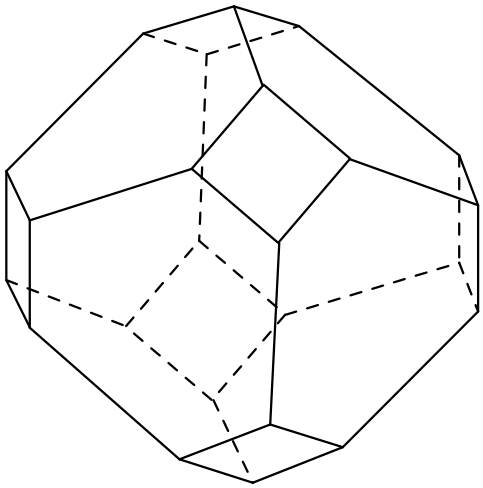

Figure 7. Optimal completed geometric figure of bound atoms forming face-centered cubic structure [59].

where n is the total number of atoms, ε_{sub} is the binding energy per atom for a bulk system, and A is the specific surface energy. The optimal shape of the crystalline particle in Fig. 7 is characterized by the maximum binding energy for a given number n of atoms, and hence by the minimal surface energy. In the case of a short-range interaction of atoms, the optimal figure is tetrakaidecahedron [60], and its facets are 6 squares and 8 regular hexagons. The specific surface energy amounts in this event to $A = 7.56$ [46, 61]. Constructing the figure of interest in a general case [59], we characterize it by the parameter

$$\delta = \frac{l_6}{l_4 + l_6}\,, \tag{3.21}$$

where l_4 is the length of a general edge of surface squares and hexagons, and l_6 is the length of the other edges of hexagons. The geometric figure under consideration (see Fig. 7) with surface squares and hexagons is realized if $0 < \delta < 1$ [59]. Table 15 enumerates the optimal values of δ and A for a crystalline particle with the Morse interaction potential between constituent atoms [58]. Note that the connection between the nearest neighbor distance a and the equilibrium distance R_{e} in the diatomic molecule is given in Table 12 in accordance with formula (3.13). One can see that a decrease in the Morse parameter, which leads to a more active role of interaction between non-nearest neighbors in the total particle energy, is accompanied by an increase both in asymmetry of the particle shape and its surface energy. For the Lennard – Jones crystalline particle, the above parameters are $\delta = 0.3$ and $A = 15.1$ [44]. As is seen, the specific surface energy in the Lennard – Jones case is twice that in the case of a short-range interaction of atoms.

We define the crystal surface tension, i.e. the surface energy per unit area, as the specific energy which is consumed when dividing a crystal into two parts. We neglect here the pressure of the equilibrium vapor over the forming surface because its value is relatively small for the solids under consideration, and then the surface tension is revealed as the specific energy consumed on breaking the bonds between atoms which belong to different parts of the particle cut. Let us determine this quantity for a short-range interaction of atoms in the crystal. According to the data of Table 15 we have $g_{100} = 2$ for $\{100\}$-surface plane and $g_{111} = 3/2$ for $\{111\}$-surface plane, and because the surface area per one atom is a^2 for the $\{100\}$ plane and $a^2\sqrt{3}/2$ for the $\{111\}$ plane, we obtain the surface tension for these planes in the form

$$\sigma_{100} = \frac{2D}{a^2}\,, \quad \sigma_{111} = \frac{D\sqrt{3}}{a^2}\,. \tag{3.22}$$

In this case the distance a between nearest neighbors coincides with the equilibrium distance R_{e} for the diatomic molecule.

On the basis of formulas (3.22) we get approximately for the surface tension of a solid with the face-centered cubic structure and a random direction of the surface:

$$\sigma_{\text{fcc}} = \frac{1.9D}{a^2}\,, \tag{3.23}$$

which is accurate to about 10%. This is approximately a half as many as in the Lennard – Jones crystal, where the surface tension is given by formula (3.18).

In conclusion of this section we note that the consideration of model systems is useful for the analysis of real systems in two respects. First, comparing the results of these models with the parameters of real systems, one can choose the model describing such a real system. In particular, the model of a system with a short-range interaction of atoms is appropriate for describing the rare gas systems in contrast to a widespread standpoint that the properties of dense and condensed rare gases are determined by the Lennard – Jones interaction potential between atoms. Second, the use of the scaling laws allows us to understand more deeply the nature of the system under consideration and acquire new data about additional parameters of the models. This will be demonstrated for models describing the liquid state of rare gas systems.

4. Phase transitions in dense systems of particles

4.1 Solid – liquid phase transition in rare gases

We now consider the solid – liquid phase transition for a system of bound atoms with a short-range interaction and pose a simple model of this phenomenon using the data for rare gases. The liquid state [62 – 66] differs from the solid one by the presence of voids inside the system. Because of the short-range character of atomic interaction in condensed rare gases, the phase transition in these systems can be analyzed on the basis of the lattice gas model for these systems [67 – 69]. Within the framework of this model, atoms are located at sites in the lattice, and only neighboring atoms interact in this lattice. If the number of sites N in this lattice is large compared to the number of atoms n, two limiting distributions exist, which in the limit $n \to \infty$ correspond to two phase states, viz. the ordered and disordered states (see Fig. 8). In the first case the atoms form a compact structure, so that each atom has practically the maximum possible number of nearest neighbors for this lattice (we denote the number of nearest neighbors for an internal site by q). Designating the energy of attraction of two neighboring atoms as ε, we obtain the quantity $q\varepsilon n/2$ for the total binding energy of the ordered state. The concentration of atoms in this lattice is $c = n/N$, and we will follow the Bragg – Williams approximation [67 – 70], thus assuming the binding energy of atoms for different random distributions of atoms over sites to be identical. This energy equals $acq\varepsilon n/2$, where the numerical factor $a \sim 1$, and the excitation energy of the disordered state is $\varepsilon nq(1 - ac)/2$.

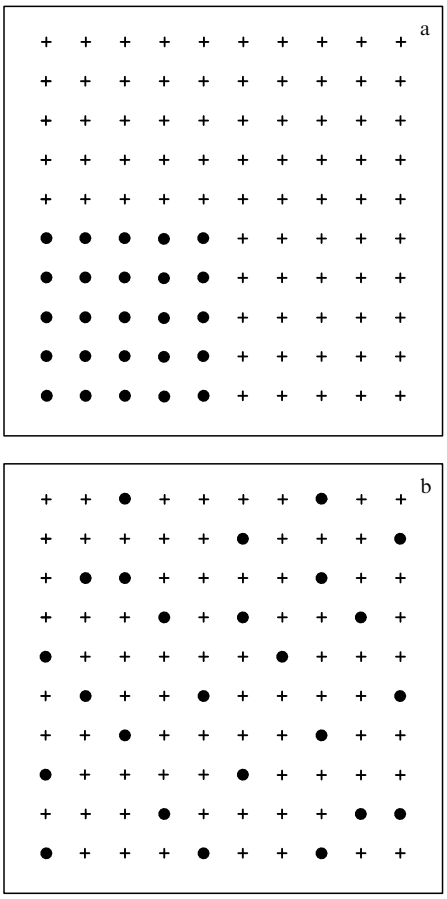

Figure 8. Distribution of atoms over sites for the lattice gas model: (a) the ordered (solid) state, and (b) the disordered (liquid) state. Crosses indicate the positions of lattice sites, and filled circles correspond to atomic positions.

The entropy of the disordered state, when atoms are distributed over sites randomly, is given by

$$S = \ln \frac{N!}{n!(N-n)!} = -N\big[c \ln c + (1-c)\ln(1-c)\big]. \quad (4.1)$$

We used the Stirling formula and the condition $N, n \gg 1$. As a result, we have for the free energy $F_{\mathrm{d}}(T)$ of the disordered state, if the free energy of the ordered state is $F_0 = 0$:

$$F_{\mathrm{d}} = E - TS = \frac{\varepsilon}{2} qn(1-ac) + TN\left[c\ln c + (1-c)\ln(1-c)\right]. \quad (4.2)$$

Whence follows the expression for the phase transition temperature T_* with due regard for the condition of the phase transition having the form $F_{\mathrm{d}} = 0$:

$$T_* = \frac{\varepsilon}{2} \frac{q(1-ac)}{\ln(1/c) + (1-1/c)\ln[1/(1-c)]}. \quad (4.3)$$

Assuming $T_* \ll \varepsilon$, we find that the order–disorder phase transition is possible for certain parameters of this model and, in particular, for a certain concentration of atoms in the given lattice.

In spite of this model being rough, one can convince oneself from this that realization of the order–disorder or solid–liquid phase transition is problematic for a system of interacting atomic particles. Hence, the presence of the phase transition gives additional information about the system. We use this fact for condensed rare gases, considering them as systems with a short-range interaction of atoms and accounting for the liquid state differs from the solid one by the presence of voids inside the system [43]. We shall prepare the liquid state of this system from the solid one in the following manner [71, 72]. Let us take a crystal consisting of n atoms and create inside it v vacancies. Then during a short time that is comparable with the typical time τ_{rel} of atomic displacement over a distance of the order of the nearest neighbor distance, the system relaxes. This relaxation leads to compression of the system and an increase of its internal energy. After a relatively long time τ_{v} voids reach the surface of this system and disappear or new voids penetrate from the surface to the system's interior. We will consider this system during times

$$\tau_{\mathrm{rel}} \ll t \ll \tau_{\mathrm{v}}, \quad (4.4)$$

when the number of voids inside the system varies weakly. So, we describe the system by the temperature T, which is connected with the kinetic energy of atoms, and the number of voids v inside it. If the system has two phase states, as do condensed rare gases, the partition function logarithm as a function of the number of voids takes a form as shown in Fig. 9. The maxima of this latter function correspond to the solid and liquid states, correspondingly.

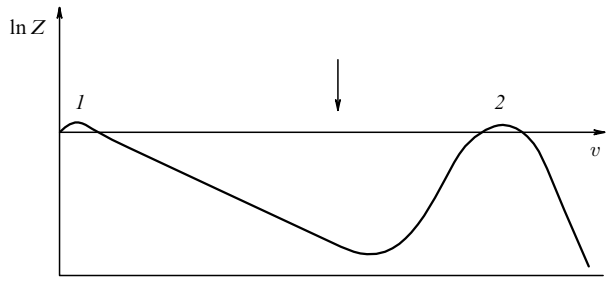

Figure 9. The dependence of the partition function logarithm for a system of bound atoms with a pair interaction on a number of vacancies. The group of states *1* corresponds to the solid state, the group of states *2* relates to the liquid state, and the arrow indicates the beginning of interaction between voids [72, 73].

Table 16 collates the values of some parameters of condensed rare gases, which follow from the data of Table 5

Table 16. Parameters of the solid and liquid states of condensed rare gases [44, 71, 72].

Parameter	Ne	Ar	Kr	Xe	Average
v_{sol}/n, 10^{-5}	3.1	1.5	1.3	1.4	1.9 ± 0.8
n/v_{liq}	3.14	3.12	3.11	3.12	3.12 ± 0.01
g	64	71	73	77	71 ± 5
$U(v_{\mathrm{liq}}/n)/D$	3.10	3.41	3.44	3.35	3.32 ± 0.15
$U(v_{\min}/n)/D$	1.20	1.32	1.35	1.30	1.29 ± 0.06
$-\ln Z(v_{\min}/n)/n$	0.7	0.39	0.40	0.40	0.39 ± 0.01
γ_{liq}	2.90	2.91	2.92	2.91	2.91 ± 0.01
$\rho_{\mathrm{ex}}/\rho_{\mathrm{liq}}$	0.879	0.866	0.876	0.871	0.873 ± 0.006
$\Delta H_{\mathrm{rel}}/D$	0.49	0.47	0.48	0.48	0.48 ± 0.01
$\sigma R_{\mathrm{e}}^2/D$	0.76	0.77	0.76	0.79	0.78 ± 0.01

and the form of the partition function logarithm in Fig. 9. In Table 16 we used the following notation: $v_{\rm sol}$ is the number of vacancies for the solid state, $v_{\rm liq}$ is the number of voids for the liquid state at the melting point, $g_{\rm v}$ is the statistical weight of an individual void, $v_{\rm min}$ is the number of voids at which the partition function Z of the system has a minimum, and U is the decrease in the energy of void formation for a given number of voids, this quantity being considered as an effective interaction potential of voids. Indeed, the energy consumed on formation of one void is $\varepsilon_{\rm sub} - U(v/n)$, where $\varepsilon_{\rm sub}$ is the specific energy of solid sublimation or the energy of formation of one vacancy in the solid. Defining an individual void as a result of development of a vacancy formed in the crystal lattice, we really give the parameters of the crystal with vacancies, which is created at the initial instant and then relaxes to the liquid state. In Table 16, $\gamma_{\rm liq}$ is the average number of nearest neighbors of a test atom, which are then removed at creation of the liquid state, $\rho_{\rm ex}$ is the density of the system at the beginning, $\rho_{\rm liq}$ is the density of the liquid state, and $\Delta H_{\rm rel}$ is the energy per atom which is released as a result of relaxation. These data are added to the model of the liquid state and we relate these parameters to a bulk system of classical bound atoms with a short-range interaction.

This microscopic approach provides the method for extracting configuration excitations in a system of bound atoms in aggregate states of this system. Fulfilling this operation for clusters where the phases can coexist, we obtain additional information about the system in a transition region, and this finding is useful for the analysis of such systems [74].

Thus, a simple model allows us to describe the character of the melting process for a bulk system of atoms with a short-range interaction, i.e. when nearest neighbors only partake in the interaction. This scheme considers the melting as the configuration excitation of the atomic system, and models such excitations by means of the formation of voids inside the system as a result of their relaxation after removal of some internal atoms from the crystal outside. The absence of equilibrium with respect to a number of voids allows us to continuously vary the number of voids, and in this way one can transit from the solid state of this atomic system to the liquid one. Condensed rare gases are real bound-atom systems with a short-range interaction between atoms, and the thermodynamic parameters of their solid and liquid states at the triple point deliver the parameters for the microscopic description of the melting process and configuration excitation of the system under consideration.

Of course, this model does not describe the variety of properties of the liquid state [57, 62 – 66, 75], but it allows us to understand the microscopic structure of the liquid. Within the framework of this microscopic description, we consider the liquid state of a system of interacting atoms as a group of excited states near the second maximum of the curve in Fig. 9 under the condition (4.4), when the time of observation is small in comparison to the lifetime of an excited state with a given number of voids inside the system (we are dealing with the configuration excitation of the system). This lifetime is connected with the transport of voids from the system's interior to its surface or vice versa. A higher time corresponds to the solid – liquid or liquid – solid transition, namely, the lifetime of supercooled liquid or superheated solid. While we ignore these transitions, one can consider the solid and liquid phase states as independent thermodynamic states [76, 77]. In this manner, one can continue the liquid phase state to low temperatures, and the solid state to high temperatures, considering them as 'cool' and 'hot' branches of the system's state [76, 77] in a wide range of parameters, including such a range where the existence of these states is not profitable thermodynamically.

Thus, the scaling analysis of the solid – liquid phase transition for condensed rare gases together with the general character of this phenomenon allows one to describe the nature of this phase transition with the use of accessible numerical parameters. Indeed, from the data of Table 5 it follows that the mechanical work done in the process of expansion during the phase transition is relatively small near the triple point, i.e. the solid – liquid transition is only determined by configuration excitation of condensed rare gases. The degree of configuration excitation is characterized by an empty space — voids inside the system. Within the framework of this consideration, the liquid state includes a group of states with different energies of configuration excitation, if the free energy of these states is close to the corresponding minimal free energy (see Fig. 9). In this way, one can understand the microscopic nature of the phase transition. Of course, this picture only relates to systems with a short-range interaction of atoms and does not reflect all the peculiarities of the phase transitions [28, 78, 79].

4.2 Phase transitions in clusters

The solid – liquid phase transition is described in the framework of classical thermodynamics, and the above statistical model permits us to understand what the aggregate state is from the microscopic standpoint. In due course, new methods and new objects arise in respect to this problem. Most progress was achieved by studying the phase transitions in clusters on the basis of computer simulation. The reason is that a cluster as a system of a finite number of bound atoms admits computer analysis better than a macroscopic system. Next, the phase transition constitutes a collective phenomenon with the participation of many atoms, and numerical computer methods are able to take them into account, in contrast to analytical methods based on a one-particle approach. In addition to this, clusters make a convenient model for a macroscopic system. Below we shall briefly describe the phase transitions in clusters.

A new property of the phase transition in clusters compared to macroscopic systems is the coexistence of solid and liquid phases [80 – 87]. This is shown in Fig. 10 where the distribution is given for the total kinetic energies of atoms composing the Lennard – Jones cluster. This cluster involves 13 atoms and has a completed icosahedral structure [88], which is illustrated in Fig. 11 [89]. An excited liquid state of the cluster is formed as a result of an atomic transition from the occupied shell to the cluster surface. Coexistence of phases means that for a certain part of the time the cluster is found in the solid state, and it spends the other part of time in the liquid state.

It is essential that cluster melting is accompanied by a change of some correlations in the cluster, which are analyzed simultaneously with an atomic motion, and these correlations are used as the characteristics of the phase transition in computer simulations. Therefore, this phenomenon is fixed reliably during the process of computer modeling. The phase transition in clusters is more complex than in ordinary macroscopic systems, and the caloric curves, i.e. the temperature dependences of the current cluster internal energies, enable one to extract several types of phase transitions

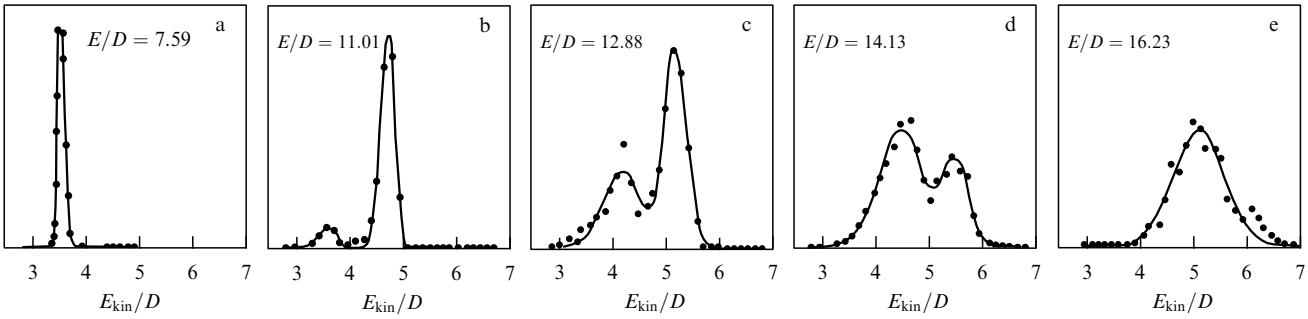

Figure 10. Distribution function for the total kinetic energy of atoms in a Lennard – Jones cluster consisting of 13 atoms. The range near the left maximum corresponds to the liquid state, and the right maximum and the range close to it relate to the solid state [80]: E is the total binding energy of atoms, and E_{kin} is the total kinetic energy of atoms.

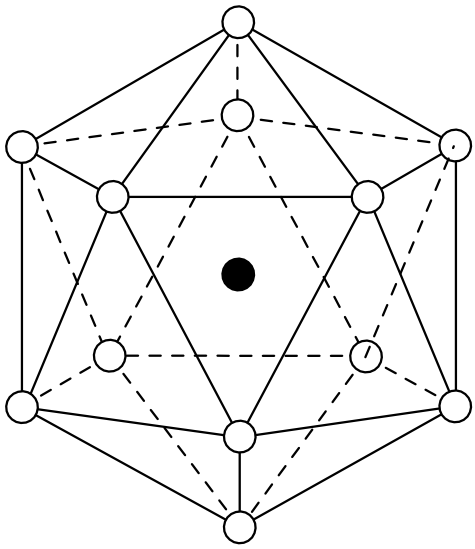

Figure 11. Icosahedral cluster consisting of 13 atoms [89].

related to the melting of different cluster shells (see, for example, Ref. [86]). As the number of cluster atoms increases and the cluster is transformed into a macroscopic system, only two types of phase transitions remain, so that the first relates to internal atoms, and the second involves surface atoms. In considering the melting of macroscopic systems, we shall concentrate on the bulk phase transition involving internal atoms.

Formation of the liquid aggregate state of a macroscopic system of atoms results in configuration excitation of the system, which consists (in the macroscopic case) in the origin of vacancies and voids inside the system. One can analyze the configuration excitation starting from the behavior of the electron energy of the system. We assume that the processes under consideration proceed without transitions between electronic states, i.e. atoms move across one electron energy surface or electron energy 'landscape'. The peculiarity of the cluster energy landscape was understood at the first stage of the numerical studies of clusters. Based on the monotonic dependence of the electron energy, one should use a simple method for the numerical evaluation of the optimal configuration of cluster atoms and the maximum binding energy of cluster atoms if, starting from an arbitrary configuration of atoms, we move atoms towards an increase in the binding atomic energy. One can expect the global minimum of the electron energy to be found in this way.

The first calculations have shown that this scheme is not realized because there are many local minima of the electron energy. For example, one of the first analyses of the Lennard – Jones cluster consisting of 13 atoms showed the existence of 988 local minima of the electron energy [90]. More detailed analysis of this system [91] revealed 1478 local minima and 17357 saddles relevant to this cluster. The number of local minima grows in an exponential fashion with an increase in the number of cluster atoms [92]. Hence, the development of a system of bound atoms as a result of motion of this system over the electron energy surface is determined by its passage through saddles and local minima of this electron surface [92, 93].

Since the electron energy surface has many local minima, and the transitions between them result from the passage through saddle points, a special formalism was developed for the analysis of the system's evolution along the electron landscape. Figure 12 illustrates the disconnectivity graph approach [94, 95] which simplifies the analysis of the cluster evolution along the electron landscape. Figure 13 gives an example of the transition between two minima of the electron energy [95]. This figure depicts the optimal path for transition between the lowest and second minima of the electron energy for a cluster consisting of 75 atoms with the Lennard – Jones interaction potential between them. As a result of the transition between these minima, the cluster passes through many local minima and saddle points of the electron energy landscape. These examples demonstrate the general character of transitions in clusters between states of configuration excitation, and these transitions result in overcoming the barriers which are saddle points of the electron energy landscape, i.e. it is convenient to consider the evolution of this system in terms of the so-called saddle-crossing dynamics [96].

Simultaneously, the above analysis throws light on the nature of the liquid state of a system of bound atoms, if the liquid state results from the configuration excitation of the solid state. Due to the saddle points of the electron energy landscape, atoms are locked between its barriers for a long time, and this character of evolution of such systems explains the short-range order for atoms in bulk liquids.

Thus, a study of the phase transitions in clusters by means of computer simulation is in progress, allowing one both to understand the nature of this phenomenon and to evaluate numerical parameters related to the thermodynamic parameters of specific clusters.

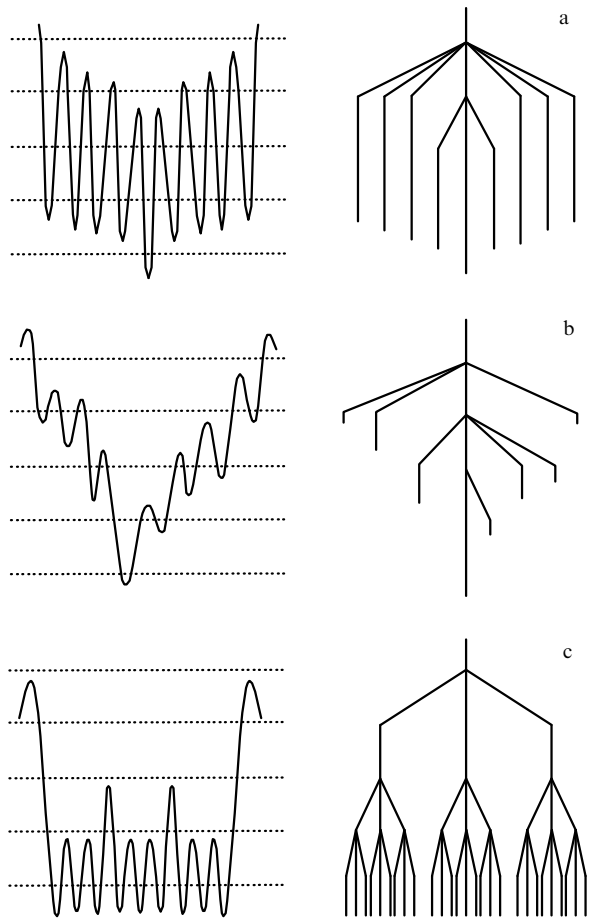

Figure 12. Method of construction of disconnectivity graphs on the basis of minima and saddle points of the electron energy surface as a function of a generalized coordinate [95]. These graphs include the principal information about the properties of the electron energy landscape.

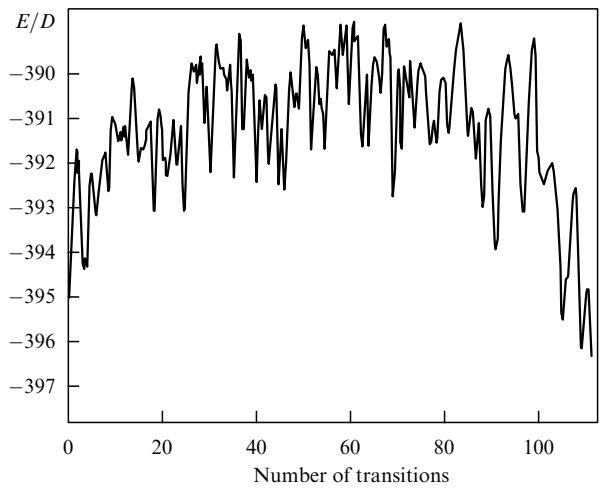

Figure 13. Shortest path for the transition between the second lowest electron energy minimum and global minimum for the cluster consisting of 75 atoms with the Lennard–Jones interaction potential [89]. This transition occurs through 65 local minima of the electron energy landscape.

4.3 Liquid state of a system of particles with a pair interaction potential

Formation of the liquid state of a system of interacting particles results from collective phenomena in this system. The liquid state can be described by various models [62–66] depending on the properties under consideration. Above we analyzed the structure of a system of interacting particles in the liquid state within the framework of a rough model (see Section 2.4): we considered the liquid state as a result of formation of vacancies at sites of a crystal lattice, and this model gave a proper connection between the specific fusion energy and a jump in the atomic density as a result of the phase transition. Of course, this model is not capable of describing the structure of the liquid state.

The more realistic model of the previous section (see Section 4.1) considers the liquid state as a mixture of interacting atoms and free voids. The parameters of each void vary in the course of its evolution, but all the voids are identical on average. In this way we describe an individual void by the average void volume, the energy consumed on formation of one void, and the statistical weight of an individual void. The formation of voids increases the volume which is accessible to classical motion of atoms, and this fact is taken into account by the void statistical weight. Though voids are independent on average, their parameters depend on the relative number of voids, and we define an individual void strictly as a result of relaxation of a vacancy. In this way on the basis of parameters of the liquid state of rare gases and from the fact of existence of the liquid state we restore the void parameters (see Table 15), and they testify about the structure of the liquid state of rare gases. As one more example, in Fig. 14 we depicted the caloric curves for argon, i.e. the temperature dependences of the specific internal energy of atoms for two aggregate states of argon. As is seen, the supercooled liquid cannot exist below the freezing temperature T_*, where the liquid maximum of the argon free energy disappears.

We now use this model for determination of the liquid surface tension. We define the surface tension σ as the specific energy which is spent in order to divide a condensed system into two parts [89, 90]. Then we represent this energy as the difference between the energy of breaking the bonds for atoms which belong to different parts of the drop cut and the energy which is released as a result of destruction of surface voids. Assuming atoms of the condensed system to be distributed randomly, on the basis of formula (3.23) we have for the surface tension

$$\sigma = \frac{1.9D}{a^2}\,\frac{q}{12} - \frac{\varepsilon_{\mathrm{v}}}{2a_{\mathrm{v}}^2} = \frac{1}{2a^2}\left[3.2D - \varepsilon_{\mathrm{v}}\left(\frac{v}{n}\right)^{2/3}\right]. \qquad (4.5)$$

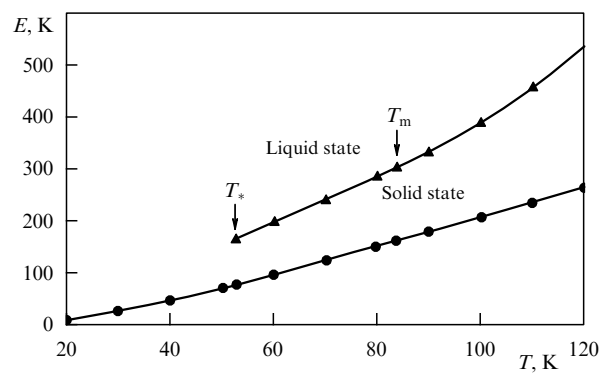

Figure 14. Caloric curves for argon — the temperature dependences of the internal energy of aggregate states.

Here, a is the average distance between nearest-neighbor atoms, a_v is the same quantity for voids, so that $a_v = a(n/v)^{1/3}$, ε_v is the energy of formation of a void, n, v are the numbers of atoms and voids, respectively, q is the number of nearest neighbors of an internal atom for the liquid state (see Table 6), and the factor $q/12$ accounts for the decrease in the number of bonds for an internal atom. In preparing Table 16 we used the relationship (4.5) with $a = R_e(\rho_0/\rho_{liq})^{1/3}$, where the required parameters were taken from Table 5. The difference between evaluated values of the surface tension and those measured (see Table 6) testifies that the accuracy of the approach under consideration is 20–40%. Formula (4.5) can be utilized for the determination of critical parameters if, as a definition of the critical point, we assume that at this point the surface tension is zero [89–91].

4.4 System of repulsing particles

Above we were dealing with a condensed system of interacting atoms, when the solid state or the ordered state of the atomic system arises as a result of attraction of neighboring atoms. We now consider the case of a high external pressure, so that the typical distance between nearest atoms meets the region of their repulsion (see Fig. 1). This corresponds to high external pressures satisfying to the criterion

$$p \gg p_0 ,$$

and we shall consider now the pressure range which is reciprocal to that analyzed in Section 2. We shall approximate the interaction potential $U(R)$ of two nearest atoms in the range of distances R between them which is responsible for the phase transition by the formula

$$U(R) = \frac{A}{R^k} , \tag{4.6}$$

and the parameters of this formula for rare gas atoms are given in Table 1. The unit of length for the system of repulsing atoms is defined as

$$d = \left(\frac{A}{T}\right)^{1/k} , \tag{4.7}$$

where T is the temperature in the melting curve. Introducing the pressure p, the specific volume jump ΔV as a result of melting, and the density ρ_{sol} for the solid state in the melting curve, we obtain the following scaling laws correct in the melting curve [101]:

$$p \sim \frac{T}{d^3} , \quad \Delta V \sim d^3 , \quad \rho_{sol} \sim \frac{1}{V} \sim \frac{1}{d^3} . \tag{4.8}$$

Note that according to the data of Table 5, the mechanical work $p_{tr}\Delta V_{tr}$ done in the course of melting near the triple point (p_{tr} is the pressure at the triple point, and ΔV_{tr} is the specific volume jump at the triple point) differs from the fusion enthalpy change ΔH_{fus} by almost four orders of magnitude. In the case of a system of repulsing particles these quantities are comparable, and the system of interest is supported by an external pressure which compels the particles to be concentrated in a restricted volume. Then, depending on the parameter values, the particles have a random or ordered distribution which conforms to the liquid or solid phase state of the system.

Table 17. Melting-curve parameters of the phase transition between the dense and rarefied aggregate states of a system involving repulsing particles with the interaction potential (4.6) [100, 101]. Here, V_d, V_r are the volumes per atom of the dense and rarefied aggregate states, correspondingly, $\Delta V = V_d - V_r$, ΔS are the jumps of the specific volume and the entropy per atom at the melting point.

k	4	6	6	12	∞
$T/(pV_d)$	0.011	0.026	0.036	0.053	0.091
$V_d\sqrt{2}/d^3$	0.254	0.641	1.030	1.185	1.359
$V_r\sqrt{2}/d^3$	0.255	0.649	1.060	1.230	1.499
$\Delta V/V_d$	0.005	0.013	0.030	0.038	0.103
$p\Delta V/T$	0.45	0.50	0.63	0.72	1.16
ΔS	0.80	0.75	0.84	0.90	1.16

In Table 17 are tabulated the parameters in the melting curve for a system of particles with the interaction potential (4.6) for different k, and in this table p, T are the pressure and temperature in the melting curve, respectively, ΔV, ΔS are the jumps of the specific volume and entropy as a result of melting, N_{sol}, N_{liq} are the number densities of particles in the solid and liquid states in the melting curve which are reduced to that of the close-packed structure ($\sqrt{2}/d^3$). According to these data, the mechanical work $p\Delta V$ done during melting is comparable with the melting heat or the fusion enthalpy $\Delta H_{fus} = T\Delta S$. However, in the limit $k \to \infty$ the melting becomes a reversible process, so that the fusion energy is compensated by the energy released in the course of the system's expansion.

From the data of Table 17 follows that the parameter $T/(pV)$ is small for a sharply varied repulsion interaction potential of atoms, thus allowing one to neglect the temperature effects in the first approximation. We shall use this fact below when establishing the connection between the pressure and the nearest neighbor distance for a given aggregate state of a system involving repulsive atoms, if we characterize this state by the average number q of nearest neighbors surrounding internal atoms. Let us use the equation of state for this atomic system, which is based on the virial theorem and has the following form [24, 28]

$$T = pV - \frac{k}{3}\,\bar{U} , \tag{4.9}$$

where V is the volume per atom, and $\bar{U}$ is the average interaction potential per atom. In the mean field approximation we arrive at the following relationships

$$V = \frac{a^3}{\sqrt{2}}\,\frac{12}{q} , \quad \bar{U} = \frac{q}{2}\,U(a) . \tag{4.10}$$

where a is the nearest neighbor distance, and the pair interaction potential $U(a)$ is defined by formula (4.6). In the limiting case $pV \gg T$, this equation gives for the pressure

$$p = 2\sqrt{2}k\left(\frac{q}{12}\right)^2 \frac{U(a)}{a^3} . \tag{4.11}$$

Let us show the validity of this formula in the case when the atoms form the close-packed crystal lattice. Let us draw a plane which is parallel to the symmetry plane of this lattice, so that the pressure represents the force per unit area acting

between atoms which are located on the different sides of the cut plane. Then the pressure is written as

$$p = \frac{mf_x}{s} = \frac{mf\cos\theta}{s}\,, \tag{4.12}$$

where m is the number of nearest neighbors for a test surface atom, which reside on the other side of the separation plane, s is the surface area per atom, f_x is the force projection onto the perpendicular to the intersecting plane, so that this force acts between a test atom and its nearest neighbor on the other side of the separation plane, f is the force itself, and θ is the angle between the line connecting interacting atoms and the perpendicular to the intersecting plane. From this we have for the $\{100\}$ cut plane ($m = 4$, $s = a^2$, $\cos\theta = 1/\sqrt{2}$):

$$p = \frac{4f(a)}{\sqrt{2}a^2} = \frac{2\sqrt{2}}{a^2}\left|\frac{\mathrm{d}U(a)}{\mathrm{d}a}\right| = \frac{2\sqrt{2}}{a^3}\,kU(a)\,. \tag{4.13a}$$

In the case of the $\{111\}$ direction of the intersecting plane we find ($m = 3$, $s = \sqrt{3}a^2/2$, $\cos\theta = \sqrt{2/3}$)

$$p = \frac{3f(a)}{\sqrt{3}a^2/2}\sqrt{\frac{2}{3}} = \frac{2\sqrt{2}}{a^2}\left|\frac{\mathrm{d}U(a)}{\mathrm{d}a}\right| = \frac{2\sqrt{2}}{a^3}\,kU(a)\,, \tag{4.13b}$$

i.e. the pressure is the same as in the previous case and coincides with that defined by formula (4.11) for $q = 12$.

4.5 Phase transition in a system of hard spheres

Let us take a look at the limiting case $k \to \infty$, which corresponds to the hard sphere model for interaction of atomic particles. In this model, the particle interaction is contact in character that simplifies the analysis, and the relative volume per atom where a particle interacts strongly with surrounding particles is small compared with the free volume per particle. Therefore, one can model atoms in this system by hard spherical particles. It is convenient to characterize the state of the particles' system by the packing density φ, and this parameter is defined as

$$\varphi = \frac{4\pi}{3}\,r^3 N\,, \tag{4.14}$$

where $r = d/2$ is the particle radius, and N is the number density of particles. Evidently, the maximum of this quantity corresponds to the crystal close-packed structure (face-centered cubic or hexagonal structure), when each particle-ball touches 12 nearest neighbors, and this parameter is equal to

$$\varphi_{\mathrm{cr}} = \frac{\pi\sqrt{2}}{6} = 0.7405\,. \tag{4.15}$$

As a result of computer modeling at large pressures, the packing density in this limit runs into [102–104]

$$\varphi_{\mathrm{d}} = 0.644 \pm 0.005 \tag{4.16}$$

and the packing density at low temperatures and high pressures tends to this limit as $\varphi_{\mathrm{d}} - \varphi \sim 1/p$ [105]. Approximately the same result follows from plain experiments [106–108] on filling a container with hard balls. By way of illustration Fig. 15 exhibits the packing density as a result of filling a container of volume V with steel balls. There are two ways of performing this operation. In the first case, the balls occupy out initial positions, and the character of such a filling is called random loose packing [109]. In the second case, the

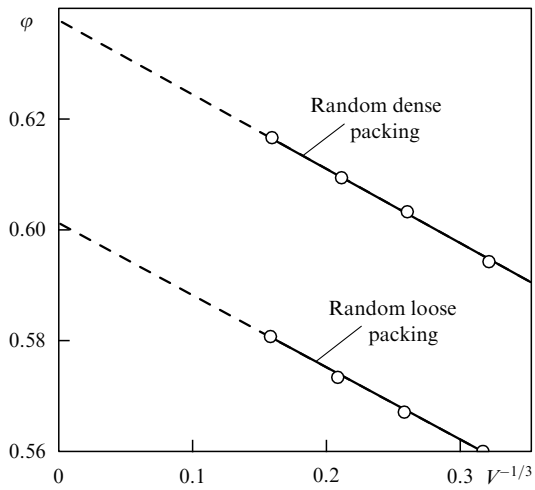

Figure 15. Dependence of the packing density on the reciprocal container size (V is the container volume) in circumstances where this volume is occupied by hard balls of identical radius for two methods of filling: with and without shaking [107].

container is shaken, and the balls combine into a more compact configuration. This operation may be improved by addition of lubricating oil to the container, and the distribution of balls is then called random dense packing [109] or the random dense configuration. Evidently, to obtain the values of the packing density for a bulk system it is necessary to take a container volume V ultimately large because surface effects may be neglected in this case. But one can also make use of several containers of finite sizes and extrapolate the packing density to an infinite size of the container. This approach is represented in Fig. 15 and gives for the packing density of a macroscopic system of balls the values $\varphi = 0.64$ and $\varphi = 0.60$ for the states of random dense packing and the random loose packing, correspondingly. Of course, the accuracy of this extrapolation is inferior to that of computer modeling. Nevertheless, this modeling may be added to the results of computer simulation and it shows the reliability of the results obtained.

The system of hard spheres admits a phase transition between its aggregate states [110, 111]. This transition is made between two random atomic distributions, which are termed as the random dense state and random loose state [109], and we will denote them by the subscripts rd and rl, correspondingly. These states are characterized by the values of the packing density $\varphi_{\mathrm{rd}} = 0.545$ and $\varphi_{\mathrm{rl}} = 0.494$ at the phase transition. Let us compare them with the data of Table 17 [101] that give in the limit $k \to \infty$:

$$\varphi_{\mathrm{d}} = \frac{\pi d^3}{6V_{\mathrm{d}}} = 0.545\,, \quad \varphi_{\mathrm{l}} = \frac{\pi d^3}{6V_{\mathrm{l}}} = 0.494\,. \tag{4.17}$$

As is seen, in both cases we obtain identical results.

Along with the above-mentioned random states of the system of hard balls, the glassy state of the latter system is also discussed [112–114] for the density of packing above the freezing density of the system. It is assumed that the glassy state of this system is stable thermodynamically [75]. The analysis [104, 105] revealed that this state can be realized only in a system with a small number of particles and, therefore, the glassy state is absent for a macroscopic system of hard particles.

We use the approach of the mean field for a system of atoms with a strongly varied potential of atomic repulsion. The state of such a system may be characterized by the coordination number q, i.e. the average number of nearest neighbors for an internal test atom, which is connected with the density ρ of a given system in any aggregate state by analogy with formula (2.12) as [37]

$$q = 24 - 12\,\frac{\rho_{\rm cr}}{\rho}\,,$$

where $\rho_{\rm cr}$ is the crystal density. We may avail ourselves of $q = 12$ for the crystal state. Evidently, in the limit $k \to \infty$, i.e. for the system of hard balls, the coordination number q is connected with the packing density φ by the formula

$$q = 24 - 12\,\frac{\varphi_{\rm cr}}{\varphi} = 24 - \frac{8.89}{\varphi}\,, \tag{4.18}$$

where $\varphi_{\rm cr}$, φ are the packing densities for the crystal state and the aggregate state under consideration, respectively, and we made use of the fact that for the crystal state $\varphi_{\rm cr} = \pi\sqrt{2}/6 = 0.7405$. Hence to the left of the melting curve at high pressures we have (the state of random dense packing) $\varphi = 0.545$ which corresponds to $q = 7.7$, and to the right of the melting curve (the state of random loose packing) where $\varphi = 0.494$ we obtain $q = 6.0$. Far from the melting curve for a dense, strongly compressed rare gas we find $q = 10.1$, i.e. this coordination number coincides with that for the liquid state of rare gases at low pressures, when such a system of bound atoms is supported by attractive forces between atoms. In addition, from the data of Table 17 follows the equation of state for a system of hard spheres ($k \to \infty$) if the pressure tends to infinity at a given temperature (the packing density is equal to $\varphi = 0.64$ in this limit):

$$\frac{pV}{T} = 9.4\,, \tag{4.19}$$

where V is the volume per atom.

We intend now to prove the suggestion that the crystal state is not realized for a system with a strongly repulsive interaction potential between atoms [115]. Let us compare the energy parameters for the crystal state of the system of repulsing atoms and a random atomic distribution which is characterized by a coordination number q. We shall analyze the possibility of the phase transition between these states taking into consideration that the number of repulsing atoms is conserved at the phase transition as well as the pressure and temperature do. Then the condition of the phase transition is formulated for the variation of the free energy: $\Delta F = 0$, where

$$\Delta F = \Delta E - T\Delta S\,,$$

and ΔE, ΔS are the changes of the internal energy and entropy. Because $p = \text{const}$, we have from formula (4.6):

$$\Delta E = n(\Delta\bar{U} + p\Delta V)\,, \tag{4.20}$$

where $\bar{U} = qU(a)$ is the average interaction energy per atom, $U(a)$ is the pair interaction potential (4.6), a is the nearest neighbor distance, and V is the volume per atom. From formula (4.11) follows the relationship governing the transition from the crystal state with $q = 12$ to another state which is characterized by a coordination number q:

$$\begin{aligned}\frac{\Delta E}{n} &= \left(1 + \frac{k}{3}\right)(\bar{U}_{\rm cr} - \bar{U}_{\rm d}) \\ &= \left(1 + \frac{k}{3}\right)\left[6U(a_{\rm cr}) - \frac{q}{2}\,U(a_{\rm r})\right] \\ &= 6U(a_{\rm cr})\left(1 + \frac{k}{3}\right)\left[1 - \frac{q}{12}\,\frac{U(a_{\rm r})}{U(a_{\rm cr})}\right],\end{aligned}$$

where $a_{\rm cr}$, $a_{\rm r}$ are the nearest neighbor distances for the crystal state and the state with a random distribution of atoms, correspondingly. Using the pressure conservation condition $p(a_{\rm cr}) = p(a_{\rm r})$ we arrive at

$$\frac{\Delta E}{n} = 6U(a_{\rm cr})\left(1 + \frac{k}{3}\right)\left[1 - \left(\frac{12}{q}\right)^{(k-3)/(k+3)}\right]. \tag{4.21}$$

From this it follows that the transition from the crystal state to any random state of the system of repulsing atoms, which is accompanied by a decrease in the nearest neighbor distance, corresponds to the situation where $\Delta E < 0$. Evidently, the transition from the crystal (ordered) state of atoms to any random (disordered) state of atoms leads to an entropy increase, $\Delta S > 0$. Hence, the crystal state of a system of repulsing atoms with a sharply varied interaction potential ($k > 3$) is not stable thermodynamically with respect to the transition into a disordered state, i.e. the state with a random distribution of atoms.

On the basis of these data we may construct the phase diagrams for rare gases [115] (see Fig. 16). At low pressures ($p \ll p_0$), the Clapeyron law gives for the melting curve near the triple point:

$$\frac{{\rm d}p}{{\rm d}T} = \frac{\Delta S}{\Delta V} = \frac{14 \pm 1}{R_{\rm e}^3}\,, \qquad p \ll p_0\,. \tag{4.22}$$

Above we used the data of Table 5 for parameters of rare gases near the triple point. This part of the melting curve corresponds to the phase transition from the crystal state ($q = 12$) to the liquid state ($q = 10.1$), and the crystal state is realized to the left from the melting curve. Another portion of the melting curve at $p > p_0$ is determined by the repulsion part

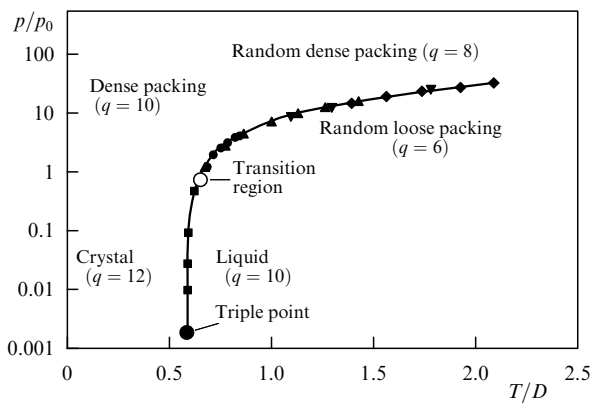

Figure 16. Phase diagram for condensed rare gases over a wide pressure range. Squares relate to the pressure range where atoms are attracted, and the parameters for this region are taken from Ref. [44]. Experimental results for argon are used in the repulsive region of the phase curve: circles — [116], up triangles — [117], down triangles — [118], and diamonds — [119].

of the interaction potential between atoms, which is approximated by formula (4.6), and for $k \gg 1$ the phase transition takes place between the states of random dense packing ($q = 7.7$) and random loose packing ($q = 6.0$). We used the experimental results [116–119] for argon on this part of the melting curve. As is seen, in the transition region of the melting curve the structure of the atomic system varies both to the left and to the right of the melting curve. To the left of the melting curve, the crystal state is realized at low pressures, and the random atomic distribution takes place at high pressures. Evidently, the transition between these states proceeds continuously, because in the opposite case we should obtain a jump in various thermodynamic parameters of the system in the course of variation of the pressure off the melting curve. This relates to the regions positioned both to the right and left of the melting curve. The above results show the complexity of the phase transition making even in simple atomic systems.

5. Condensed and dense molecular gases

5.1 System of ball-like molecules

One can expand the scaling analysis elaborated for the case of dense and condensed rare gases to molecular systems. As for rare gases, one can construct a similar scaling law for round molecules. This was made for a bound system of fullerene molecules C_{60} in paper [120]. The fullerene molecule has the form of a truncated icosahedron, so that the molecular surface is made up of 12 pentagons and 8 hexagons [121, 122]. If these molecules form a crystal, the phase transition proceeds at the temperature 257 K [123, 124] and above this temperature the bound molecules can freely rotate being located at sites of the crystal lattices. Then the interaction between fullerene molecules is governed by a pair interaction potential averaged over molecular orientations. In this case we face a full analogy with the case of condensed rare gases [125]. This analogy allowed the restoration of the unknown parameters of condensed and dense fullerene systems on the basis of the scaling analysis [120].

The same scheme can be used for the systems composed of round molecules if the interaction between these molecules weakly depends on molecular orientations. This takes place at not too low temperatures, when molecules can freely rotate in a system of bound molecules. Table 18 contains the parameters of dense and condensed systems of tetrafluoride molecules which are an example of ball-like molecules. The values which were found on the basis of the scaling laws are given in parentheses. Though the accuracy of the scaling law in this case is worse than in the case of dense and condensed rare gases, it is estimated as about 10%. This figure also characterizes the accuracy of the parameters restored. In addition, the ratio of quantities of an identical dimensionality for these molecular systems may differ from that of rare gas systems.

One more peculiarity of molecular systems relates to the boiling point which is defined as the temperature at which the saturated vapor pressure reaches 1 atm. But the reduced pressure depends on the parameters of the system considered, and therefore usage of the boiling point as a scaling parameter of the system becomes problematic. Nevertheless, in the case of rare gases this approach is valid because the triple point pressure is significantly less than 1 atm. But in the case of molecular gases this rule can be violated. Moreover, in the cases of SF_6 and UF_6 systems their melting points are higher than the boiling points, i.e. the boiling takes place from the solid phase. Note also the absence of the scaling law for the fusion energy ΔH_{fus} of these systems, thus indicating a different character of the phase transition for these systems.

We consider tetrafluoride molecules as ball-like molecules, so that the systems consisting of these molecules must be identical to those of rare gas atoms. But comparison of the data from Table 9 and Table 18 shows that the identity between these systems is only partial. In particular, the ratio $V_{\text{cr}}/V_{\text{liq}} = 2.70 \pm 0.06$ for rare gas systems corresponds to $V_{\text{cr}}/V_{\text{liq}} = 2.8 \pm 0.1$ for systems of tetrafluoride molecules, and the parameter combination $T_{\text{cr}}/(p_{\text{cr}} V_{\text{cr}}) = 3.4 \pm 0.1$ for rare gas systems coincides with the value of $T_{\text{cr}}/(p_{\text{cr}} V_{\text{cr}}) = 3.6 \pm 0.1$ for systems of tetrafluoride molecules within the

Table 18. Parameters of dense and condensed systems of metal – tetrafluoride and SF_6 molecules.

Parameter	MoF_6	SF_6	UF_6	WF_6	IrF_6	ReF_6	Average
T_{m}, K	291	223	338	276	317	292	—
T_{b}, K	307	209	330	290	327	307	—
T_{cr}, K	473	319	506	444	(500)	(470)	—
ε_{ev}, meV	282	236	394	268	316	293	—
ε_{liq}, meV	350	247	442	274	357	364	—
ΔH_{fus}, meV	45	52	200	42	87	—	—
p_{cr}, MPa	4.75	3.77	4.66	4.34	(8)	(4.6)	—
V_{cr}, $\text{cm}^3\,\text{mol}^{-1}$	226	199	250	233	(140)	(240)	—
a, 10^5 MPa $\text{cm}^6\,\text{mol}^{-2}$	(13)	7.86	16.0	13.2	(9)	(14)	—
b, $\text{cm}^3\,\text{mol}^{-1}$	(100)	88	113	106	(63)	(110)	—
ρ_{liq}, g cm^{-3}	2.6	1.9	4.7	3.4	6.0	3.6	—
V_{liq}, $\text{cm}^3\,\text{mol}^{-1}$	81	77	75	88	51	83	—
$T_{\text{cr}}/T_{\text{m}}$	1.62	1.43	1.50	1.61	(1.58)	(1.61)	1.54 ± 0.09
$T_{\text{cr}}/T_{\text{b}}$	1.54	1.52	1.53	1.53	(1.53)	(1.53)	1.53 ± 0.01
$\varepsilon_{\text{ev}}/T_{\text{b}}$	10.7	13.1	13.8	10.7	11.2	11.1	12 ± 1
$\varepsilon_{\text{ev}}/\varepsilon_{\text{liq}}$	0.81	0.96	0.89	0.98	0.88	0.80	0.89 ± 0.07
$\varepsilon_{\text{ev}}/T_{\text{cr}}$	6.9	8.6	9.0	7.0	—	—	8 ± 1
$T_{\text{cr}}/(p_{\text{cr}} V_{\text{cr}})$	3.66	3.53	3.61	3.65	—	—	3.6 ± 0.1
V_{liq}/b	—	0.87	0.85	0.83	—	—	0.85 ± 0.02
V_{cr}/b	—	2.26	2.21	2.20	—	—	2.22 ± 0.03
$V_{\text{cr}}/V_{\text{liq}}$	2.8	2.6	3.3	2.7	—	—	2.8 ± 0.3
$\Delta H_{\text{fus}}/\varepsilon_{\text{ev}}$	0.16	0.22	0.51	0.16	0.27	—	0.26 ± 0.14

limits of the accuracy of these values. This means that the expansion of the systems in the course of their transition from the triple point to the critical point is identical for these system types. But the ratio ε_{ev}/T_{cr} is different for these systems, which indicates a different character of interaction accompanying these phenomena. Notice that the data used in Table 18 have a restricted accuracy, which speaks for increasing the error in the scaling analysis.

5.2 System of diatomic molecules

Constructing the scaling laws for rare gases, we based our consideration on two parameters of the pair atomic interaction potential: R_e and D. Because the interaction potential between molecules is anisotropic and depends on the orientation of molecules, the number of base parameters increases, and the usage of scaling laws for molecular systems is problematic. The accuracy of this operation can be found using the results of the analysis itself. In contrast to the rare gas systems, it is convenient to take the parameters of these systems as basic parameters for the scaling analysis of molecular systems instead of the parameters of the pair interaction potential between molecules. The reliability of such a scaling scheme shows an increase because the number of physical parameters used for molecular systems is more than three, i.e. the number of dimensional parameters which form the basis of the dimensional analysis. Next, we divide the molecular systems into groups with identical structures of molecules, and analyze the scaling laws inside a separate group. This increases the accuracy of the analysis. In addition, using the scaling analysis for molecular systems, we can find unknown parameters for some systems on the basis of the same parameters for other systems. This inference is more important now than in the case of rare gas systems.

We will now look at the systems consisting of diatomic molecules which contain identical atoms. These molecules can form gases under certain conditions. We shall exclude hydrogen as a quantum system from the consideration and restrict ourselves to classical systems only, where the scaling analysis is simpler. Table 19 contains parameters of dense and condensed molecular systems involving diatomic molecules. We use the same notation for parameters of molecular systems as for the parameters of dense and condensed rare gases. From the data of Table 19 one can estimate the degree of validity of the scaling laws for the systems under consideration and ascertain the peculiarities of this analysis as applied to molecular systems.

It should be emphasized that diatomic molecules form crystal lattices of other structures than the close-packed ones, so that the properties of crystals of diatomic molecules differ from those of the close-packed structure. In particular, as follows from Table 19, the scaling law for the fusion energy ΔH_{fus} relevant to systems of diatomic molecules is characterized by an accuracy of one order of magnitude worse than in the case of rare gas systems or for other parameters of Table 19. Thus, it is better to use the parameters of liquid and gaseous molecular systems for the scaling analysis, i.e. the parameters of liquids and dense gases along with critical parameters.

5.3 Dense and condensed freons and halomethanes

The systems of bound molecules can have additional properties which influence the structure and parameters of their condensed systems. As an example, we shall consider a bound system of halomethane molecules. The basis of these molecules is formed by the methane molecule having a carbon atom in the center and where the hydrogen atoms compose a tetrahedron. Some or all the hydrogen atoms can be replaced by fluorine or chlorine atoms in the halomethane molecules under consideration. We assume these molecules to be classical in a bound system and different halomethane molecules to have an identical structure in condensed molecular systems.

This inference may be violated because some halomethane molecules have a dipole moment, and the interaction between dipole moments of molecules can change the structure of the crystal lattice consisting of these molecules. In the limiting case when the dipole–dipole interaction of molecules dominates, these molecules form a body-centered cubic crystal lattice. Below we shall consider this limiting case and, assuming molecules to form the body-centered cubic crystal lattice, evaluate the binding energy per molecule due to the dipole–dipole interaction between molecules in such a

Table 19. Parameters of dense and condensed systems of diatomic molecules.

Parameter	F_2	N_2	O_2	Cl_2	Br_2	I_2	Average
T_m, K	53.53	63.29	54.36	172.1	265.9	386.0	—
T_b, K	85.03	77.34	90.2	239.1	331.9	457.5	—
T_{cr}, K	144.1	126.2	154.6	416.9	588.1	819.1	—
ε_{liq}, meV	76	62	78	232	330	468	—
ε_{ev}, meV	67.9	57.8	70.6	211	311	432	—
ΔH_{fus}, meV	53	7.5	4.6	66	112	158	—
ρ_{liq}, g cm^{-3}	1.52	0.88	1.14	1.51	3.12	(2.7)	—
ρ_{sol}, g cm^{-3}	—	1.03	2.00	2.03	4.05	4.93	—
p_{cr}, MPa	5.18	3.39	5.04	7.99	10.3	(12)	—
p_{liq}, 10^3 MPa	3.5	1.1	2.5	9	11	15	—
V_{cr}, cm^3 mol^{-1}	66	90	73	123	127	155	—
a, 10^5 MPa cm^6 mol^{-2}	1.17	1.37	1.38	6.34	9.75	—	—
b, cm^3 mol^{-1}	29.0	38.7	31.9	54.2	59.1	(70)	—
T_{cr}/T_m	2.69	2.00	2.84	2.43	2.21	2.12	2.4 ± 0.3
T_{cr}/T_b	1.70	1.63	1.71	1.74	1.77	1.79	1.72 ± 0.06
$T_{cr}/(p_{cr}V_{cr})$	3.5	3.4	3.5	3.5	3.7	—	3.5 ± 0.1
$\varepsilon_{ev}/\varepsilon_{liq}$	0.89	0.93	0.90	0.91	0.94	0.92	0.92 ± 0.02
V/b	—	0.35	0.25	0.32	0.33	—	0.31 ± 0.04
ε_{ev}/T_{cr}	5.5	5.3	5.3	5.9	6.1	6.1	5.7 ± 0.4
V_{cr}/b	2.28	2.32	2.29	2.27	2.15	—	2.26 ± 0.06

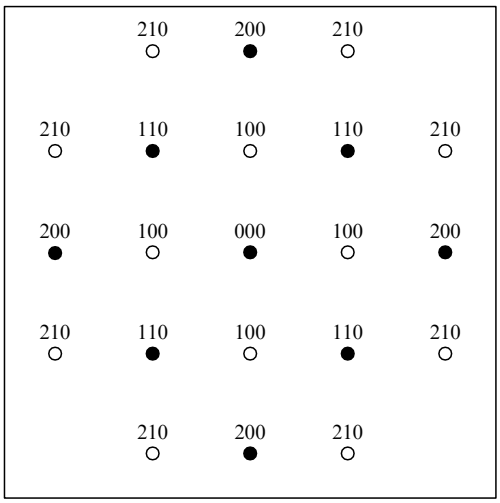

Figure 17. Positions and directions of molecular dipole moments in the crystal lattice of the body-centered cubic structure which is established due to the dipole – dipole interaction of molecules. The shell is indicated, where a given molecule is located. The molecular dipole moments are directed perpendicular to the drawing plane, and their two directions are indicated by filled and open circles. The other lattice layers are parallel to this picture and have the same positions of molecules and directions of their dipole moments.

crystal. Comparing this value with that of $\varepsilon_{\rm liq}$, following from the temperature dependence of the saturated vapor pressure (2.6), one can ascertain the role of the dipole – dipole interaction in the formation of a crystal lattice.

Evidently, in the limiting case under consideration it is profitable for each molecule to have nearest neighbors with the opposite direction of the dipole moment on the plane which is perpendicular to the direction of the dipole moments as illustrated in Fig. 17. The same positions of molecules and directions of their dipole momenta relate to neighboring planes which are parallel to this one. The interaction potential between the dipole moments of two molecules is equal to

$$V(r) = \frac{\mathbf{d}_1\mathbf{d}_2 - 3(\mathbf{d}_1\mathbf{n})(\mathbf{d}_2\mathbf{n})}{r^3}\,, \tag{5.1}$$

where $\mathbf{d}_1$, $\mathbf{d}_2$ are the dipole moments of molecules, r is the distance between molecules, and $\mathbf{n}$ is the unit vector along the line connecting molecules. Let us take a test molecule and evaluate the total energy of its interaction with other molecules. This quantity will determine a contribution to the binding energy per molecule due to the dipole – dipole interaction between molecules, and according to formula (5.1) it is equal to

$$U_{\rm dip} = \frac{1}{2}\sum_k n_k V(r_k)\,. \tag{5.2}$$

Here we distributed molecules of the crystal lattice over shells around a test molecule similar to the approach taken in Section 3.1 for other lattice types; r_k is the distance of a test molecule from molecules of the kth shell, and n_k is the number of molecules for the kth shell. One can represent this formula, in view of relationship (5.1), in the form

$$U_{\rm dip} = \frac{1}{2}\sum_k c_k\,\frac{d^2}{r_k^3}\,, \tag{5.3}$$

Table 20. Parameters of shells of the body-centered cubic lattice and dipole – dipole interaction between molecules of these shells and a test molecule.

Shell	r_k^2/a^2	Layer	n_k	Parity*	c_k
100	1	0	4	–	–4
		±1	2	+	–4
110	2	0	4	–	+4
		±1	8	+	+4
111	3	±1	8	–	0
200	4	0	4	+	–4
		±2	2	+	+4
210	5	0	8	–	–8
		±1	8	–	–16/5
		±2	8	–	56/5

* The parity has sign +, if the molecular dipole moment direction coincides with that of a test molecule, and sign – for the opposite direction.

where d is the molecular dipole moment, and the values of c_k are given in Table 20 together with some other parameters. The molecular shells are conveniently divided into subshells, so that for molecules of one subshell all the parameters of formula (5.2) are identical. Each shell in Table 20 is denoted by the reduced coordinates x, y, z of molecules fallen into this shell, where $x \geqslant y \geqslant z$, and the unit of length is the lattice constant a, i.e. the nearest neighbor distance of the body-centered cubic lattice.

From the data of Table 20 we obtain for the binding energy per molecule due to the dipole – dipole interaction the following result:

$$U_{\rm dip} = 2.6\,\frac{d^2}{a^3} = 2.6Nd^2\,, \tag{5.4}$$

where N is the number density of molecules in the crystal, and a is the nearest neighbor distance. Table 21 contains the values of the interaction energy per molecule $U_{\rm dip}$ for the body-centered cubic lattice with the directions of molecular dipole moments introduced according to Fig. 17. As is seen, this quantity is small compared to the real binding energy $\varepsilon_{\rm liq}$ for these molecules, where the binding energy was obtained on the basis of formula (2.6) for the temperature dependence of the saturated vapor pressure. Though this binding energy relates to the liquid state of the molecular systems, it can be used for estimates. As a result of comparison, for all the cases one finds $\varepsilon_{\rm liq} > U_{\rm dip}$. Of course, we make use of the dipole moments of isolated molecules, while in condensed systems

Table 21. Binding energy and dipole – dipole interaction in halomethane crystals.

Molecule	$\varepsilon_{\rm liq}$, meV	ρ, g cm^{-3}	N, 10^{22} cm^{-3}	d, D	$U_{\rm dip}$, meV
CF_4	140	1.62	1.34	0	0
CF_3Cl	163	—	—	0.50	—
CF_2Cl_2	227	1.64	0.82	0.51	35
$CFCl_3$	273	1.50	0.66	0.46	23
CCl_4	348	1.59	0.62	0	0
CHF_3	191	1.52	1.31	1.65	58
CH_2F_2	223	0.91	1.05	1.98	84
CH_3F	206	0.58	1.03	1.86	58
CH_4	102	0.466	1.75	0	0
CH_3Cl	247	0.92	1.10	1.89	64
CH_2Cl_2	340	1.33	0.94	1.60	39
$CHCl_3$	424	1.48	0.75	1.04	13

Table 22. Parameters of fluorine – chlorine methanes and methane systems.

Parameter	CF_4	CF_3Cl	CF_2Cl_2	$CFCl_3$	CCl_4	CH_4	Average
T_m, K	89.3	(137)	115	(214)	250	90.6	—
T_b, K	145	191.7	243.3	296.8	349	111.6	—
T_{cr}, K	228	302	385	471.3	556	191	—
ε_{liq}, meV	140	163	227	273	348	102	—
ε_{ev}, meV	127	(143)	203	(240)	311	85	—
p_{cr}, MPa	3.7	3.9	4.1	4.4	4.6	4.60	—
p_{liq}, 10^3 MPa	8	1.6	5.3	3.9	3.9	5.2	—
V_{cr}, cm^3 mol^{-1}	136	180	217	250	280	99	—
V_{liq}, cm^3 mol^{-1}	54	—	74	92	97	34	—
a, 10^5 MPa cm^6 mol^{-2}	4.0	6.9	10.7	14.7	20.1	2.30	—
b, cm^3 mol^{-1}	63	81	100	111	128	43.0	—
T_{cr}/T_m	2.5	—	2.1	—	2.2	2.1	2.2 ± 0.2
T_{cr}/T_b	1.57	1.58	1.58	1.59	1.59	1.71	1.60 ± 0.05
ε_{liq}/T_{cr}	7.1	6.3	6.8	6.7	7.3	6.2	6.7 ± 0.4
$\varepsilon_{ev}/\varepsilon_{liq}$	0.91	—	0.89	—	0.89	0.83	0.88 ± 0.03
V_{cr}/b	2.16	2.22	2.17	2.25	2.19	2.30	2.22 ± 0.05
V_{liq}/b	0.86	—	0.74	0.83	0.76	0.79	0.80 ± 0.05
$T_{cr}/(p_{cr}V_{cr})$	3.8	3.6	3.6	3.6	3.6	3.5	3.6 ± 0.1

they can increase as a result of atomic displacement by virtue of interaction. In any case, for freons, i.e. halomethane molecules with fluorine and chlorine atoms substituting the hydrogen atoms, the dipole – dipole interaction is relatively small, and we consider separately the systems of these molecules in Table 22.

Collecting the parameters of halomethane molecules in Table 22, we consider them as an example of ball-like molecules, so that in crystals they form a lattice of close-packed structure. Molecules containing simultaneously fluorine and chlorine atoms have different sizes in the direction of the dipole moment and perpendicular to it, but we neglect this fact. Parameter values obtained on the basis of the scaling analysis are given in parentheses. One can see that the reduced parameters of systems involving these molecules coincide within the limits of their accuracy with those of Table 18 for the systems of tetrafluoride molecules.

Summing up the results of this section, we notice that the scaling analysis allows us to restore unknown parameters of molecular systems on the basis of known parameters. The accuracy of this operation for liquid and gaseous systems is about 10%. As for the solid molecular systems, their scaling-based results require additional analysis and in some cases may be not correct. In addition, the scaling analysis of molecular systems uses the parameters of these systems as the basic ones.

6. Conclusions

The scaling analysis made for rare gas and molecular systems allows us to express the parameters of these systems through three basic parameters. In the case of rare gases, the basic parameters comprise the atomic mass m, the equilibrium distance R_e between atoms and the depth D of the potential well in the pair interaction potential. The analysis of rare gas systems shows that their properties near the triple point and critical point, some parameters of the solid and liquid states, the properties of a dense gas and the parameters of a saturated vapor above the solid and liquid surfaces can be expressed through these basic parameters of rare gases with an accuracy of several percent. This means that all these properties are determined by the attractive part of the interaction potential of atoms, and the long-range interaction between atoms gives a minor contribution to various parameters of dense and condensed rare gases, as also are quantum effects.

Being spread to molecular systems, the scaling analysis conserves the main conclusions drawn for systems of rare gas atoms. As basic dimensional parameters, along with the molecular mass, it is convenient to employ the parameters of the gaseous and liquid phases, in particular, the parameters of the critical point. The scaling approach allows one to restore unknown parameters of molecular systems on the basis of three basic parameters for a given molecular system. The statistical error of this operation is estimated at $\sim 10\%$ if one relies on the above analysis for molecular systems.

The scaling analysis can be spread to various molecular systems where the molecules conserve their individuality. The requirements for the character of interaction in these systems are such that a long-range interaction between molecules is not important, and one can neglect the quantum effects. The experience acquired from the above analysis proves the validity of these requirements for real molecular systems within the limits of the accuracy peculiar to these data. But if the molecular systems of a given group are characterized by different structures of the crystal lattice, the scaling analysis is valid only for the liquid and gaseous parameters of such systems.

The scaling method lends aid in the choice of suitable models for the description of real systems of interacting atoms or molecules. In addition, it helps to develop the existing models for these systems and to understand more deeply the nature of some properties and phenomena inherent in the systems under consideration. Some examples of this approach were considered above, and a variety of other properties can also be analyzed in this way.

References

1. Sena L A *Edinitsy Fizicheskikh Velichin i Ikh Razmernosti* (Units of Physical Quantities and Their Dimensions) (Moscow: Nauka, 1977) [Translated into English (Moscow: Mir Publ., 1972)]
2. Sedov L I *Metody Podobiya i Razmernosti v Mekhanike* (Similarity Methods and Dimensionalities in Mechanics) (Moscow: Nauka, 1977) [Translated into English: *Similarity and Dimensional Methods in Mechanics* (Moscow: Mir Publ., 1982)]
3. Okun' L B *Fizika Elementarnykh Chastits* (Physics of Elementary Particles) (Moscow: Nauka, 1984)

4. McCoubrey A O *Guide for the Use of the International System of Units* (Gaithersburg, M.D.: NIST, 1991)
5. Landau L D, Lifshitz E M *Gidrodinamika* (Fluid Mechanics) (Moscow: Nauka, 1988) [Translated into English (Oxford: Pergamon Press, 1986)]
6. Krainov V P *Qualitative Methods in Physical Kinetics and Hydrodynamics* (New York: American Institute of Physics, 1992)
7. *American Institute of Physics Handbook* (Coord. Ed. D E Gray) (New York: McGraw-Hill, 1972)
8. Vargaftik N B *Spravochnik po Teplofizicheskim Svoĭstvam Gazov i Zhidkosteĭ* (Tables on the Thermophysical Properties of Liquids and Gases) 2nd ed. (Moscow: Nauka, 1972) [Translated into English (Washington: Hemisphere Publ. Corp., 1975)]
9. Moses A J *The Practicing Scientist's Handbook* (New York: Van Nostrand Reinhold Co., 1978)
10. Reid R C, Prausnitz J M, Poling B E *The Properties of Gases and Liquids* 4th ed. (New York: McGraw-Hill, 1987)
11. Rabinovich V A *Thermophysical Properties of Neon, Argon, Krypton, and Xenon* (Washington: Hemisphere Publ. Corp., 1988)
12. Emsley J *The Elements* 2nd ed. (Oxford: Clarendon Press, 1991)
13. Barin I *Thermochemical Data of Pure Substances* 2nd ed. (Weinheim: VCH, 1993)
14. *Handbook of Chemistry and Physics* (Ed. D R Lide) 79th ed. (London: CRC Press, 1998 – 1999)
15. Aziz R A, Slaman M J *Chem. Phys.* **130** 187 (1989)
16. Aziz R A, Slaman M J *J. Chem. Phys.* **92** 1030 (1990)
17. Dham A K et al. *Mol. Phys.* **67** 1291 (1989)
18. Dham A K et al. *Chem. Phys.* **142** 173 (1990)
19. Dalgarno A *Adv. Chem. Phys.* **12** 143 (1967)
20. Leonas V B *Usp. Fiz. Nauk* **107** (3) 29 (1972) [*Sov. Phys. Usp.* **15** 266 (1972)]
21. Schilling H *Statistische Physik in Beispielen* (Leipzig: Fachbuchverlag, 1972)
22. Sivukhin D V *Obshchiĭ Kurs Fiziki* (General Course of Physics) Vol. 2 *Termodinamika i Molekulyarnaya Fizika* (Thermodynamics and Molecular Physics) (Moscow: Nauka, 1975)
23. Stauffer D, Stanley H E *From Newton to Mandelbrot: A Primer in Theoretical Physics* (Berlin: Springer-Verlag, 1990)
24. Hirschfelder J O, Curtiss Ch F, Bird R B *Molecular Theory of Gases and Liquids* (New York: Wiley, 1954)
25. Zharkov V N, Kalinin V A *Uravneniya Sostoyaniya Tverdykh Tel pri Vysokikh Davleniyakh i Temperaturakh* (The State Equations of Solids at High Pressures and Temperatures) (Moscow: Nauka, 1968) [Translated into English: *Equations of State for Solids at High Pressures and Temperatures* (New York: Consultants Bureau, 1971)]
26. Leontovich M A *Vvedenie v Termodinamiku. Statisticheskaya Fizika* (Introduction to Thermodynamics. Statistical Physics) (Moscow: Nauka, 1983) [Translated into German: *Einführung in die Thermodynamik* (Hochschulbücher für Physik, Bd. 6) (Berlin: Deutscher Verlag der Wissenschaften, 1953)]
27. Ter Haar D, Wergeland H *Elements of Thermodynamics* (Reading, Mass.: Addison-Wesley Publ. Co., 1966)
28. Landau L D, Lifshitz E M *Statisticheskaya Fizika* (Statistical Physics) Vol. 1 (Moscow: Nauka, 1976) [Translated into English (Oxford: Pergamon Press, 1980)]
29. Honig R E, Hook H O *RCA Rev.* **21** 360 (1960)
30. Bunn Ch *Crystals* (New York: Acad. Press, 1964)
31. Leibfried G *Gittertheorie der Mechanischen und Thermischen Eigenschaften den Kristallen* (Berlin: Springer-Verlag, 1965) Handbuch VII, Teil 2
32. Ashcroft N W, Mermin N D *Solid State Physics* (New York: Holt, Rinehart and Wilson, 1976)
33. Kittel Ch *Introduction to Solid State Physics* (New York: Wiley, 1986)
34. Schuberth E, Creuzburg M, Müller-Lierheim W *Phys. Status Solidi B* **76** 301 (1976)
35. Bostanjonglo O, Kleinschmidt B *Z. Phys. A* **21** 276 (1977)
36. Sonnenblick Y et al. *Chem. Phys. Lett.* **52** 276 (1977)
37. Smirnov B M *Usp. Fiz. Nauk* **164** 1165 (1994) [*Phys. Usp.* **37** 1079 (1994)]
38. Smirnov B M *Phys. Scripta* **58** 595 (1998)
39. Simon F E, Glatzel G *Z. Anorg. Allg. Chem.* **178** 309 (1929)
40. Baĭdakov V G, in *Obzory po Teplofizicheskim Svoĭstvam Veshchestv* (Reviews of Thermophysical Properties of Substances) No. 69 (Moscow: IVTAN, 1988)
41. Baĭdakov V G *Mezhfaznaya Granitsa Prostykh Klassicheskikh i Kvantovykh Zhidkosteĭ* (Interface of Simple Classical and Quantum Liquids) (Ekaterinburg: Nauka, 1994)
42. Ino S *J. Phys. Soc. Jpn.* **27** 941 (1969)
43. Reiss H, Frish H L, Lebowitz J L *J. Chem. Phys.* **31** 369 (1959)
44. Smirnov B M *Clusters and Small Particles: in Gases and Plasmas* (New York: Springer-Verlag, 2000)
45. Schwentner N, Koch E-E, Jortner J *Electronic Excitations in Condensed Rare Gases* (Berlin: Springer-Verlag, 1985)
46. Smirnov B M *Usp. Fiz. Nauk* **163** (10) 29 (1993) [*Sov. Phys. Usp.* **36** 933 (1993)]
47. Pauli W *Meson Theory of Nuclear Forces* (Princeton: IAS, 1946)
48. Bethe H A, Morrison P *Elementary Nuclear Theory* 2nd ed. (New York: Wiley, 1956)
49. Smirnov B M *Usp. Fiz. Nauk* **162** (1) 112 (1992) [*Sov. Phys. Usp.* **35** 37 (1992)]
50. Smirnov B M *Usp. Fiz. Nauk* **162** (12) 97 (1992) [*Sov. Phys. Usp.* **35** 1052 (1992)]
51. Doye P K, Wales D J, Berry R S *J. Chem. Phys.* **103** 4234 (1995)
52. Fano U, Fano L *Physics of Atoms and Molecules* (Chicago: Univ. of Chicago Press, 1972)
53. Kihara T, Koba S *J. Phys. Soc. Jpn.* **7** 348 (1952)
54. Corti D S et al. *Phys. Rev. E* **55** 5522 (1997)
55. Kofke D A *J. Chem. Phys.* **98** 4149 (1993)
56. Barker J A, Henderson D *Rev. Mod. Phys.* **48** 587 (1976)
57. Martynov G A *Fundamental Theory of Liquids* (Bristol: A. Hilger, 1992)
58. Smirnov B M, Strizhev A Yu, Berry R S *J. Chem. Phys.* **110** 7412 (1999)
59. Wang S W, Falicov L M, Searcy W *Surf. Sci.* **143** 609 (1984)
60. Raoult B et al. *Philos. Mag. B* **60** 881 (1989)
61. Smirnov B M *Zh. Eksp. Teor. Fiz.* **108** 1151 (1995) [*JETP* **80** 1151 (1995)]
62. Frenkel' Ya I *Kineticheskaya Teoriya Zhidkosteĭ* (Kinetic Theory of Liquids) (Moscow: Izd. AN SSSR, 1945) [Translated into English (Oxford: Clarendon Press, 1946)]
63. Fisher I Z *Statistical Theory of Liquids* (Chicago: Univ. of Chicago Press, 1964)
64. Egelstaff P A *An Introduction to the Liquid State* (London: Academic Press, 1967)
65. Ubbelohde A R *The Molten State of Matter* (Chichester: Wiley, 1978)
66. Hansen J P, McDonald I R *Theory of Simple Liquids* (London: Academic Press, 1986)
67. Huang K *Statistical Mechanics* (New York: Wiley, 1963)
68. Feynman R P *Statistical Mechanics* (Reading, Mass.: W.A. Benjamin, 1972)
69. Ziman J M *Models of Disorder* (Cambridge: Cambridge Univ. Press, 1979)
70. Bragg W, Williams H J *Proc. R. Soc. London Ser. A* **150** 552 (1935)
71. Smirnov B M *Neorg. Mater.* **35** 672 (1999) [*Inorgan. Mater.* **35** 562 (1999)]
72. Smirnov B M, in *Nucleation Theory and Applications: Research Workshop, Dubna, Russia, April 1999* (Eds J W P Schmelzer, G Röpke, V B Priezzhev) (Dubna: JINR, 1999)
73. Smirnov B M *Zh. Eksp. Teor. Fiz.* **112** 1847 (1997) [*JETP* **85** 1010 (1997)]
74. Berry R S , Smirnov B M *J. Chem. Phys.* **114** 6816 (2001)
75. Debenedetti P G *Metastable Liquids* (Princeton, N.J.: Princeton Univ. Press, 1996)
76. Vorob'ev V S *Zh. Eksp. Teor. Fiz.* **109** 162 (1996) [*JETP* **82** 85 (1996)]
77. Vorob'ev V S *Teplofiz. Vys. Temp.* **34** 397 (1997)
78. Brout R *Phase Transitions* (New York: W.A. Benjamin, 1965)
79. Stanley H E *Introduction to Phase Transitions and Critical Phenomena* (New York: Oxford Univ. Press, 1971)
80. Berry R S, Jellinek J, Natanson G *Phys. Rev. A* **30** 919 (1984)
81. Jellinek J, Beck T L, Berry R S *J. Chem. Phys.* **84** 2783 (1986)
82. Berry R S et al. *Adv. Chem. Phys.* **70** 75 (1988)
83. Wales D J, Berry R S *J. Chem. Phys.* **92** 4283 (1990)

84. Wales D J *Chem. Phys. Lett.* **166** 419 (1990)
85. Cheng H-P, Berry R S *Phys. Rev. A* **45** 7969 (1992)
86. Kunz R E, Berry R S *Phys. Rev. E* **49** 1895 (1994)
87. Berry R S *Nature* **393** 212 (1998)
88. Mackay A L *Acta Crystallogr.* **15** 916 (1962)
89. Khanna S N, Jena P *Phys. Rev. Lett.* **69** 1664 (1992)
90. Hoare M R, Pal P *Adv. Phys.* **20** 161 (1971)
91. Ball K D, Berry R S *J. Chem. Phys.* **111** 2060 (1999)
92. Stillinger F H, Weber T A *Phys. Rev. A* **25** 978 (1982)
93. Berry R S, in *Theory of Atomic and Molecular Clusters* (Ed. J Jellinek) (Berlin: Springer-Verlag, 1999) p. 1
94. Becker O M, Karplus M *J. Chem. Phys.* **106** 1495 (1997)
95. Wales D J et al. *Adv. Chem. Phys.* **115** 1 (2000)
96. Komatsuzaki T, Berry R S *J. Chem. Phys.* **110** 9160 (1999)
97. Rusanov A I *Fazovye Ravnovesiya i Poverkhnostnye Yavleniya* (Phase Equilibria and Surface Phenomena) (Leningrad: Khimiya, 1967)
98. Rowlinson J S, Widom B *Molecular Theory of Capillarity* (Oxford: Clarendon Press, 1982)
99. Domb C *The Critical Point* (London: Taylor & Francis, 1996)
100. Stichov S M *Usp. Fiz. Nauk* **114** (6) 3 (1974) [*Sov. Phys. Usp.* **17** 625 (1975)]
101. Hoover W G, Gray S G, Johnson K W *J. Chem. Phys.* **55** 1128 (1971)
102. Berryman J G *Phys. Rev. A* **27** 1053 (1983)
103. Song Y, Stratt R M, Mason E A *J. Chem. Phys.* **88** 1126 (1988)
104. Rintoul M D, Torquato S *Phys. Rev. Lett.* **77** 4198 (1996)
105. Rintoul M D, Torquato S *Phys. Rev. E* **58** 532 (1998)
106. Bernal J D *Nature* **183** 141 (1959)
107. Scott G D *Nature* **188** 908 (1960)
108. Bernal J D, Mason J *Nature* **188** 908 (1964)
109. Gutzow I, Schmelzer J *The Vitreous State* (Berlin: Springer-Verlag, 1995)
110. Hoover W G, Ree F H *J. Chem. Phys.* **49** 6252 (1968)
111. Reiss H, Hammerich A D *J. Phys. Chem.* **90** 6252 (1986)
112. Speedy R J *J. Chem. Phys.* **100** 6684 (1994)
113. Yeo J *Phys. Rev. E* **52** 853 (1995)
114. Van Blaaderen A, Wiltzius P *Science* **270** 1177 (1995)
115. Berry R S, Smirnov B M *Zh. Eksp. Teor. Fiz.* **120** 889 (2001) [*JETP* **93** 541 (2001)]
116. Van Vitzenburg W, Stryland J C *Can. J. Phys.* **46** 811 (1968)
117. Crawford R K, Daniels W B *Phys. Rev. Lett.* **21** 367 (1968)
118. Stishov S M, Fedosimov V I *Pis'ma Zh. Eksp. Teor. Fiz.* **14** 326 (1971) [*JETP Lett.* **14** 217 (1971)]
119. Cheng V M, Daniels W B, Crawford R K *Phys. Lett. A* **43** 109 (1973)
120. Vorob'ev V S, Eletskii A V *Chem. Phys. Lett.* **254** 263 (1996)
121. Kroto H W et al. *Nature* **318** 162 (1985)
122. Kroto H *Science* **242** 1139 (1988)
123. Heiney P A et al. *Phys. Rev. Lett.* **66** 2911 (1991)
124. Tse J S, King D D, Wilkinson D A *Chem. Phys. Lett.* **183** 378 (1991)
125. Eletskiĭ A V, Smirnov B M *Usp. Fiz. Nauk* **165** 977 (1995) [*Phys. Usp.* **38** 935 (1995)]